A new chronostratigraphic anchor for the early Cambrian: Integrating δ^{13} C 1 chemostratigraphy and Bayesian astrochronology in West Gondwana (Anti-2 Atlas, Morocco) 3 4 Damien Pas^{1,2}, Matthias Sinnesael³, Kamal Mghazli⁴, Valentin Jamart¹, Gerd Geyer⁵, Ed 5 Landing⁶, Nasrrddine Youbi^{4,7,8}, Jihane Ounar⁴, Hamdi Omar^{9,10}, Moulay Ahmed Boumehdi^{4,7}, 6 Jarno J.C. Huygh², Da Silva Anne-Christine², Allison C. Daley¹, 7 8 ✓ **Damien Pas** [damien.pas@unil.ch] 9 10 (1) Institute of Earth Sciences (ISTE), University of Lausanne, Lausanne, Switzerland 11 12 (2) SediCClim, Geology Department, Liège University, Liège, Belgium (3) Geology, School of Natural Sciences, Trinity College Dublin, The University of Dublin, 13 14 Ireland (4) Department of Geology, Faculty of Sciences-Semlalia, Cadi Ayyad University, Marrakesh, 15 16 Morocco. (5) Lehrstuhl für Geodynamik und Geomaterialforschung, Institut für Geographie und 17 Geologie, Universität Würzburg, Germany 18 (6) New York State Museum, 222 Madison Avenue, Albany, NY 12230, USA 19 (7) Instituto Dom Luiz, Faculdade de Ciências, Universidade de Lisboa, 1749-016 Lisboa, 20 21 Portugal (8) Faculty of Geology and Geography, Tomsk State University, 36 Lenin Avenue, Tomsk 22 634050, Russia 23 (9) Department of Atmospheric, Oceanic, and earth Sciences, George Mason University, 24 Fairfax, VA 22030, USA 25 (10)Department of Geology, Ghent University, Krijgslaan 281 -S 8, B-9000 Gent, Belgium 26 27 28 **ORCID** Damien Pas https://orcid.org/0000-0002-2235-1974 29 Matthias Sinnesael https://orcid.org/0000-0003-0354-8250 30 Kamal Mghazli https://orcid.org/0000-0002-3987-5125 31

https://orcid.org/0000-0002-7153-0709

https://orcid.org/0000-0003-3904-0432

https://orcid.org/0000-0001-8103-3960

Valentin Jamart

Gerd Geyer

Ed Landing

32

33

Naserrddine Youbi https://orcid.org/0000-0003-3466-2400 35 https://orcid.org/0009-0006-5544-6544 36 Jihane Ounar Hamdi Omar https://orcid.org/0000-0001-8033-7401 37 Moulay Ahmed Boumehdi https://orcid.org/0000-0001-5084-1551 38 Jarno J.C. Huygh https://orcid.org/0000-0002-9171-7589 39 Da Silva Anne-Christine https://orcid.org/0000-0003-4191-7600 40 https://orcid.org/0000-0001-5369-5879 41 Daley Allison 42 43 **Abstract** The early Cambrian represents a critical interval in Earth's history characterized by rapid biological 44 45 innovation and significant perturbations in global carbon cycling. However, a comprehensive understanding of the processes at play and their spatial and temporal relationships is hindered by fossil 46 47 provincialism, diachronous bioevents, and inadequate high-precision geochronology. The Tiout section (Anti-Atlas, Morocco) offers a unique opportunity to address these challenges as it is a continuous 48 1205 m-thick succession of sedimentary rocks with multiple volcanic ash beds, together with the 49 lowest occurrence (LO) of determinable, mineralized trilobites and a refined biostratigraphy in West 50 Gondwana. In this study, we present new high-resolution $\delta^{13}C_{carb}$ stratigraphy, coupled with portable 51 XRF elemental geochemistry and Bayesian astrochronology, to refine the temporal framework of this 52 lower Cambrian succession. The Tiout δ^{13} C_{carb} record captures multiple global excursions, including 53 the termination of the Shiyantou Carbon Isotope Excursion (SHICE), excursions II and III, and the 54 55 early Atdabanian/Repinaella Zone Excursion (EAREZE or excursion IV), which has been commonly 56 confused with the Cambrian Arthropod Radiation Excursion (CARE). Cyclostratigraphic analysis of the detrital SiO₂ proxy combined with U-Pb-dates confirms previous interpretation of an eccentricity-57 58 precession origin for the decameter-scale rhythmic alternations between lighter-colored marlstones and 59 darker limestones expressed in the weathering profile. The EAREZE peak below the LO of determinable trilobites is dated at 520.046 ± 0.097 Ma. The Tiout section provides a robust, multi-60 proxy reference for a potential Global Stratotype Section and Point (GSSP) for Cambrian Series 2. 61 62 63 64 65 66 67 68 69

Table of contents: 70 71 72 1. Introduction 73 Global significance of the early Cambrian Biostratigraphic and geochronologic challenges 74 The EAREZE excursion as a correlation tool 75 76 The Tiout section as a reference locality 77 2. Materials and Methods 78 2.1. Stratigraphic framework: lithology and biostratigraphy 79 2.2. Section measurement and sampling strategy 2.3. Elemental geochemistry (pXRF) 80 2.4. Stable isotope geochemistry ($\delta^{13}C_{carb}$, $\delta^{18}O$) 81 82 2.5. Spectral analysis and Bayesian age modeling 3. Results and Discussion 83 84 3.1. Stratigraphic architecture and geochemical records of the Tiout section 3.2. $\delta^{13}C_{carb}$ stratigraphy and correlation of excursions (SHICE, II, III, EAREZE) 85 86 3.3. Identification of orbital forcing in detrital proxies 3.4. Astronomical calibration for the Tiout section 87 3.5. Bayesian astrochronology: new age constraints for Cambrian events 88 3.6. Implications for the timing of early Cambrian biogeochemical events in west Gondwana 89 3.7. Evaluation of the EAREZE (Excursion IV) as a global chronostratigraphic marker 90 91 4. Conclusions 92 5. Acknowledgements 93 6. Supplementary materials 7. Reference list 94 95 8. Figures (Figs 1-7) and Table 1 96 97 98 99 100 101 102

Introduction

- The early Cambrian (Terreneuvian–Cambrian Series 2, ~539–506.5 million years ago, Cohen
- et al. (2013) represents a transformative interval in Earth's history marked by rapid biological
- innovation, the diversification of complex life, and major shifts in global biogeochemical
- 108 cycles (Bowring et al., 1993; Peng et al., 2012; dos Reis et al., 2015; Daley et al., 2018;
- Linnemann et al., 2019; Paterson et al., 2019; Bowyer et al., 2022; Potin and Daley, 2023;
- 110 Alexander et al., 2025). The emergence of skeletonized metazoans, such as trilobites and
- archaeocyaths, fundamentally restructured marine ecosystems (e.g., Wood et al., 1992) with
- the development of complex trophic interactions and modified sediment dynamics (e.g.,
- 113 <u>Bottjer et al., 2000; Mángano and Buatois, 2017</u>). These evolutionary events occurred in
- tandem with pronounced fluctuations in the carbon cycle recorded as global δ^{13} C excursions
- that reflect changes in ocean chemistry, primary productivity, and organic carbon burial
- (Maloof et al., 2005; Maloof et al., 2010; Fan et al., 2011; Young, 2015; Betts et al., 2018;
- Holmes et al., 2025). Understanding the timing, nature, and drivers of these biogeochemical
- changes is crucial for reconstructing Earth's early biosphere and environmental dynamics.
- 119 Correlating these events on a global scale remains challenging due to the complex interplay of
- regional depositional environments, diagenetic overprints, strong biotic endemism (e.g.,
- 121 <u>Sdzuy et al., 1999; Geyer and Shergold, 2000; Landing et al., 2013a; Peng et al., 2020)</u>, and
- the limited but growing number of available high-precision radioisotope ages (Landing et al.,
- 123 <u>1998; Zhu et al., 2006b; Peng et al., 2020; Landing et al., 2023</u>). In this context, integration of
- carbon isotope stratigraphy with biostratigraphy, radioisotope ages and astrochronology is key
- for synchronizing stratigraphic successions across paleocontinents (Fan et al., 2011; Cramer
- and Jarvis, 2020; Zhao et al., 2022; Farrell et al., 2025).
- Yet, despite these advances, a central issue remains unresolved: the formal criterion for
- defining the base of the Cambrian Stage 3, corresponding with the Terreneuvian–Cambrian
- Series 2 boundary. Traditionally, this boundary has been placed at or near to the LO (lowest
- occurrence) of trilobites (Geyer and Shergold, 2000; Shergold and Geyer, 2003; Peng et al.,
- 131 <u>2012; Zhang et al., 2017</u>). This horizon is typically termed the "First Appearance Datum"
- 132 (FAD) of trilobites, but the designation FAD should be limited to a horizon marking the
- phyletic origin of trilobites and which will not be found in the course of field and laboratory
- work (Landing et al., 2013a; Aubry, 2015). In addition, the FAD horizon is further obscured in
- field settings as the earliest trilobites likely originated and diversified as non-mineralized
- forms well before the mineralization of trilobites with onset of a calcite sea (e.g., Paterson et
- 137 <u>al., 2019; Landing et al., 2024).</u>

While trilobite-based biostratigraphy remains a powerful regional correlation tool, its 138 139 application as a global chronostratigraphic marker at the base of Cambrian Series 2 is considerably undermined by the diachronous nature of the LO of mineralized trilobites 140 between paleocontinents (Geyer and Shergold, 2000; Hollingsworth, 2005a; Peng and 141 Babcock, 2011; Landing et al., 2013a; Landing et al., 2018). Their limited facies distribution 142 and endemism further complicate the use of a trilobite LO ("FAD") as a globally synchronous 143 144 marker. Consequently, alternative criteria have been proposed to serve as a GSSP marker for 145 146 Cambrian Stage 3. These include the FADs of small shelly fossils (SSFs; e.g., Mobergella 147 radiolata (Rozanov et al., 2011) or Pelagiella subangulata (Steiner et al., 2011) = 148 Pseudopelagiella subangulata sensu (Landing et al., 2021a)), acritarch species (e.g., Skiagia ornata; Moczydłowska and Zang (2006)), and, most notably, a globally recognizable δ¹³C 149 150 positive excursion termed excursion IV or CARE (Magaritz et al., 1986; Kirschvink et al., 1991; Magaritz et al., 1991; Zhu et al., 2004; Maloof et al., 2005; Dilliard et al., 2007; 151 152 Landing et al., 2013a; Landing and Kouchinsky, 2016; Betts et al., 2018; Peng et al., 2020). 153 This peak has been linked to widespread oceanographic and ecological transformations during 154 the Stage 2–3 transition (Alexander et al., 2025) and is increasingly regarded as an important feature in the global correlation of this boundary (Landing and Kouchinsky, 2016; Zhang et 155 al., 2017; Landing et al., 2021b). However, the "type" CARE was chosen for sections on the 156 157 South China paleocontinent where it lies approximately at the levels of the Chengjiang and Qingjiang biotas (Zhu et al., 2006b; Fu et al., 2019). Thus, biostratigraphic evidence indicates 158 that the CARE postdates carbon isotope excursion IV on the Siberian Platform, which has 159 been mistakenly identified as the CARE. This confusion has contributed to continuing debate 160 over its precise stratigraphic position, reproducibility, and association with biotic events 161 (Landing et al., 2013a; Zhang et al., 2017; Geyer, 2019a). To overcome this confusion, Geyer 162 (2019a) suggested the term EAREZE (Early Atdabanian/Repinaella Zone Excursion), which 163 is applied herein. Stage boundaries within the Cambrian System have proven particularly 164 165 difficult to ratify by the International Union of Geological Sciences: one series and four of the ten stages are still undefined, underscoring the need for continuous, fossiliferous, and 166 167 radiometrically dated sections that record multiple independent chronostratigraphic signals to 168 confidently select a Global Boundary Stratotype Section and Point (GSSP). The Tiout section in the western Anti-Atlas of Morocco offers a rare opportunity to satisfy the 169 170 requirements. It includes multiple volcanic zircon ID-TIMS U-Pb ages (Compston et al., 1992; 171 Landing et al., 1998; Maloof et al., 2005; Maloof et al., 2010; Landing et al., 2021b) and records

the LO of mineralized, identifiable trilobites in West Gondwana, which belong to the bigotinids 172 173 (such as *Hupetina antiqua*) and the fallotaspidids (such as *Eofallotaspis tioutensis*) along with archaeocyaths and brachiopods that enable a precise biostratigraphical scheme (Geyer, 2019b). 174 175 However, it must be emphasized that unidentifiable trilobite fragments have long been known to occur ca. 40 m lower in the lower Igoudine Formation (Geyer and Landing, 1995, 2006). 176 177 Cyclostratigraphic analysis of the Tiout section by Sinnesael et al. (2024) demonstrated that the meter-scale lithological cyclicity observed in the section by Monninger (1979) reflects an 178 astronomical origin, primarily controlled by precession and short eccentricity (~20–100 kyr) 179 180 cycles. The integration of these individual astronomical cycles with available U-Pb geochronology into a Bayesian age-depth model provided a refined age estimate for the LO of 181 182 unidentified trilobite remains in West Gondwana (519.70-519.54 Ma 95% highest posterior 183 distribution). 184 In addition to its biostratigraphic and geochronologic significance, the Tiout section also holds potential for global chemostratigraphic correlations. Preliminary low-resolution δ^{13} C_{carb} 185 186 profiles from Tiout (Tucker, 1986; Kirschvink et al., 1991) revealed a distinct positive δ¹³C_{carb} excursion, peaking in the lower member of the Igoudine Formation and below the LO of the 187 188 identifiable trilobites, but within the range of trilobites as indicated by small fragments of sclerites (Geyer, 2019c). This excursion was correlated with excursion IV in the Repinaella 189 Zone of the lower Atdabanian Stage in Siberia (Brasier and Cowie, 1989; Latham and Riding, 190 1990; Kirschvink et al., 1991). This correlation is supported by the high-resolution $\delta^{13}C_{carb}$ 191 profile obtained from the nearby Oued Sdas section that is stratigraphically equivalent to the 192 Tiout section, where a comparable positive $\delta^{13}C_{carb}$ shift is recorded (Maloof et al., 2005; fig. 193 2; Maloof et al., 2010; Landing et al., 2021b). 194 As part of ongoing efforts to address global correlation challenges at the base of Cambrian 195 Series 2, we generated a new high-resolution geochemical dataset including $\delta^{13}C_{carb}$ 196 chemostratigraphy and bulk-rock portable x-ray fluorescence (pXRF) elemental data through 197 the 1205-meter-thick continuous sedimentary succession at Tiout. This work aims to clarify 198 the structure, magnitude, and stratigraphic position of the peak of the EAREZE $\delta^{13}C_{carb}$ 199 positive excursion in relation to the LO of identifiable trilobite remains and co-occurring U-200 Pb zircon ages at Tiout. We also use pXRF-derived detrital proxies, together with $\delta^{13}C_{carb}$ 201 chemostratigraphy, biostratigraphy, and U-Pb geochronology, to build a Bayesian 202 203 astrochronological age-depth model that improves temporal resolution and enables more robust global correlations of early Cambrian successions. Finally, we discuss and integrate 204 205 those new West Gondwana results in global context and provides methodological guidance

along with our perspective for establishing Global Boundary Stratotype Sections and Points 206 207 (GSSPs). 208 209 2. Materials and method 210 2.2 Geological Background 211 During the early Cambrian, the Anti-Atlas of Morocco was part of the western margin of 212 Gondwana. It is commonly portrayed as located at ~60° South (Fig. 1; Scotese, 2021). 213 However, evaporitic minerals in the Adoudou Formation and development of carbonate 214 platform deposits with archaeocyath-microbial mound developments in the Igoudine and 215 Amouslek formations are evidence of a low latitude, tropical environment consistent with a 216 217 counterclockwise rotation of Gondwana in the Cambrian (McKerrow et al., 1992; Landing et al., 2022; Keppie et al., 2024). 218 The Tiout section, situated along the northern edge of the Anti-Atlas, is a continuous and 219 expanded marine succession that extends from the lowest Cambrian (Terreneuvian) into 220 Series 2. The composite succession, as documented by Monninger (1979), records a total 221 222 thickness of ~1600 m and encompasses the upper portion of the Adoudou, Lie de vin, Igoudine (including the Tiout Member), and Amouslek formations (Fig. 1A). The following 223 provides a summary of litho- and biostratigraphy. For a detailed overview of the regional 224 225 geology of the Anti-Atlas we refer to El Kabouri et al. (2025). The Lie de vin Formation (Choubert, 1953) is composed of cyclically interbedded siltstones 226 227 and limestones, including microbialites such as stromatolites and thrombolites and evaporite 228 pseudomorphs that indicate a restricted shallow marine paleoenvironment. At Tiout, this formation reaches up to 940 m in thickness and contains various trace fossils such as 229 (sub)horizontal burrows and U-shaped burrows identified as Diplocraterion (Latham and 230 Riding, 1990). The formation also records several dated ash beds (e.g., Ti 566, 521.06 \pm 0.12 231 Ma (see Landing et al., 2021b for the most recent works). Key ash beds within time-232 equivalent Lie de vin deposits exposed at Oued Sdas approximately 25 km east of Tiout have 233 also been radiometrically dated by Maloof et al. (2010) including the tuff M234, yielding a 234 weighted mean U–Pb zircon age of 523.17 ± 0.16 Ma (Landing et al., 2021b), that anchors the 235 lowermost part of the Lie de vin in the terminal Terreneuvian Series. 236 The overlying Igoudine Formation (Geyer, 1989) records a transition from restricted to more 237 238 open-marine conditions. At Tiout, the formation reaches a thickness of ~300 m (Geyer,

2019c). It is subdivided into a lower unnamed member (~185 m) composed of black

laminated limestones and dolosiltites, interpreted as having been deposited under dysoxic to anoxic conditions and an upper Tiout Member (~115 m) characterized by oolitic and fossiliferous grainstone representing wave-agitated shoals (Geyer and Landing, 2006; Geyer, 2019c). Fossils in the lower unnamed member include *Hyolithellus* tubes and poorly preserved undetermined trilobite sclerites (Sdzuy and Geyer, 1988; Geyer and Landing, 1995), while the Tiout Member contains a diverse fauna of early skeletal metazoans, such as trilobites (Eofallotaspis, Fallotaspis, various bigotinids), archaeocyaths, hyoliths, and chancelloriids (Debrenne and Debrenne, 1978; Sdzuy, 1978; Debrenne and Debrenne, 1995; Geyer and Landing, 1995; Geyer, 2019c). The abrupt appearance of mineralized trilobite sclerites in this interval is attributed to a shift in taphonomic or environmental conditions, with perhaps a change to a calcite ocean, rather than reflecting a true evolutionary radiation (Geyer, 2019c). The Amouslek Formation is ~260 m-thick at Tiout and records a clear but gradual transition from a carbonate-dominated setting (Igoudine Formation) to siliciclastic mudstones, indicative of further marine deepening. The contact with the underlying Igoudine Formation is a regional sequence boundary, marked by a volcanic tuff dated to 519.23 ± 0.14 Ma (Ti-Amo.0; Landing et al., 2021b)—placing it near the top of the Fallotaspis plana Zone and the base of the Choubertella Zone (Geyer, 2019b; Landing et al., 2021b).

2.1 Section measurement and sampling strategy

In this study, we systematically measured and sampled a 1205-meter-thick stratigraphic succession extending from the lower Lie de vin Formation to the lower Amouslek Formation. A total of 744 samples were collected at approximately 1.5-meter intervals. The composite section was divided into ten intervals defined by lithologic markers, linked by using lithologic markers and drone imagery (Fig. 2; Fig. S1). Key marker beds, including ash layers and the LO of trilobites, were precisely identified and located in the succession during fieldwork. Drone imagery facilitated an accurate evaluation of potential astronomically-forced climatic cycles in these lower Cambrian strata, which are several hundred meters thick and must be seen from a broader perspective to identify potential bundling. The limited vegetation cover in the area is an important parameter that allows for such a survey. Drone imagery also served as an integrative tool: it documented formation boundaries that are not easily identifiable when standing on the outcrop itself, enabled precise location of measured intervals, and allowed location of key marker beds, such as volcanic ash layers and the LO of trilobites in the section, previously identified by field observation (Fig. 3). These images were also critical for

field planning as they enabled efficient selection of the most continuous and accessible stratigraphic intervals for detailed logging and sampling, and they will continue as a reference for future field work.

2.3. Elemental geochemistry (pXRF)

All collected samples were cut using a circular saw to create a flat surface and to remove potential weathered material. Samples were then measured with a pXRF spectrometer Bruker Tracer 5g (Liège University, Belgium) equipped with the following parameters: 4 Watt, 200 µA and 50 keV X-Ray Rhodium source, a 1µm graphene window, resulting in a resolution <140 eV at 250 000 cps. Measurements were performed in dry air conditions (i.e., normal conditions without specific gas flow), using an 8 mm collimator and an acquisition time of 70 seconds, which is considered suitable to get accurate pXRF data (De Winter et al., 2017; Da Silva et al., 2023). All major and trace element data were generated using the GeoExploration internal quantification protocol and are expressed in wt.%. The full dataset is provided in Supplemental Material File 1.

2.4. Stable isotope geochemistry (δ^{13} C_{carb}, δ^{18} O_{carb})

455 samples were measured at an average 3-m resolution for the Lie de vin Formation and $\sim \! 1.5$ m resolution for the Igoudine and Amouslek formations for carbonate carbon and oxygen stable isotopes ($\delta^{13}C_{carb}$ and $\delta^{18}O_{carb}$). Aliquots of the rock powders were reacted with 100% phosphoric acid at 70°C using a Gasbench II connected to a Thermo Fisher Delta V Plus mass spectrometer at the University of Erlangen (Germany). All values are reported in per mil relative to the Vienna Pee Dee Belemnite limestone standard (VPDB). Reproducibility and accuracy were monitored by replicate analysis of laboratory standards calibrated by assigning a $\delta^{13}C_{carb}$ of +1.95% to NBS19 and -47.3% to IAEA-CO9 and a $\delta^{18}O_{carb}$ of -2.20% to NBS19 and -23.2% to NBS18. Reproducibility for $\delta^{13}C_{carb}$ and $\delta^{18}O_{carb}$ was better than $\pm 0.04\%$ and $\pm 0.10\%$ (1 std. dev.), respectively. Replicate analyses of NBS 19 were used for quality control of the measurements.

2.5. Spectral analysis and Bayesian age modeling

To detect and interpret potential Milankovitch cycles, time-series analysis was conducted on the detrital SiO₂ records measured using pXRF (Fig. 4). The numerical interpretations were cross-validated with field observations and high-resolution drone imagery, which provided essential context for stratigraphic continuity and lithological cyclicity. Time-series analysis

was conducted using different tools including Continuous Wavelet Transform (CWT) as 308 provided in the "WaverideR" R package (Arts et al., 2024) and Taner bandpass filtering, 309 Hilbert transform, and multi-taper method (MTM) as provided in the "Astrochron" R package 310 311 (Meyers, 2019). Time-series analysis script is available in Supplemental Material File S2. We constructed an integrated Bayesian age-depth model for the Tiout section by combining 312 high-precision CA-ID-TIMS U-Pb zircon geochronology with cyclostratigraphic constraints 313 derived from the floating astronomical timescale built on the interpreted short eccentricity 314 cycles. This approach was implemented using OxCal version 4.4 (Ramsey, 2009), which 315 316 relates stratigraphic depth, expressed in interpreted short-eccentricity cycles to time under the 317 assumption of a constant but unknown sediment accumulation rate following the framework 318 of Sinnesael et al. (2024) but adapted to incorporate the precise sedimentological and geochronological succession of the Tiout composite. To represent the floating astronomical 319 320 time scale, we expressed stratigraphic depth as units of interpreted short-eccentricity cycles of 321 20–40 m-thick rhythmic bundles expressed in drone-based imagery and supported by CWT 322 and MTM spectral analysis of the log₁₀-transformed SiO₂ time series. These cycles were 323 interpreted to reflect the ~110 kyr component of Earth's eccentricity, based on their bundling 324 and spectral expression. A prior distribution for ~110 kyr cycle duration was assigned as a normal distribution with a mean of 110 kyr and one standard deviation of 7.5 kyr. 325 This differs from the approach of Sinnesael et al. (2024) who adopted a shorter short 326 eccentricity cycle duration (mean of 96.5 kyr, $\sigma = 2$ kyr) derived from the time differences 327 between successive maxima in full numerical orbital solution (Lantink et al., 2022). Our 328 329 longer 110 kyr prior was intended to accommodate such practical sources of stratigraphic uncertainty as decimeter- to meter-scale horizons of cycle boundaries and minor hiatuses. We 330 331 assumed a constant sediment accumulation rate within each short eccentricity cycle and no 332 significant depositional hiatuses within the stratigraphic interval modeled. The depth model served as a reference framework to assign stratigraphic positions. We first established a depth 333 model from our field measurements, which provided the reference framework to place all 334 335 stratigraphic markers, including radiometric age constraints, the levels of the EAREZE and excursions II and III peaks, and the lowest occurrence (LO) of identifiable trilobites. At this 336 337 stage, the framework is depth-only, without a floating age model applied. To convert depth into time, we then integrated our new SiO₂-based cyclostratigraphic dataset, which allowed 338 339 recognition of eccentricity-scale cyclicity. This cyclostratigraphic model is anchored by highprecision U-Pb zircon ages from interbedded bentonitic ashes (M234, Ti566, Ti-Am-0.0). 340 341 Volcanic zircons were interpreted as syndepositional with negligible reworking. Age

uncertainties are reported as 95% highest posterior density (HPD) intervals. Full model priors,

OxCal code, and posterior outputs are provided in Supplementary File S2.

344345

346

343

3. RESULTS AND DISCUSSIONS

3.1. Lithostratigraphic correlation and framework of the Tiout section

- 347 The composite stratigraphic framework of the Tiout section presented in Figure S1 is based on
- ten laterally correlated intervals spanning a total of 1204.5 m in stratigraphy that brackets the
- 349 Lie de vin, Igoudine, and Amouslek formations. Stratigraphic continuity between measured
- partial sections that comprise the entire Tiout section was ensured with drone imagery, which
- 351 helped in the precise tracing of key lithological contacts at the top/bottom of measured
- intervals. The complete stratigraphy can be visualized in a composite image created from a
- series of drone photographs (Fig. 2B). Formation boundaries were confidently identified in
- 354 the field based on consistent differences in color, weathering profiles, and distinctive
- lithological characteristics as described in Monninger (1979), Geyer and Landing (2006) and
- 356 Landing et al. (2019).

357358

3.2. δ¹³C_{carb} stratigraphy of the Tiout section

- The δ^{13} C_{carb} profile from the Tiout section (Fig. 3) captures a continuous, well-preserved signal
- through more than a one kilometer of lower Cambrian strata. Measured δ^{13} C_{carb} values range
- 361 from -6% to +4% (VPDB), averaging near 0%, and capture major global excursions, including
- the termination of the SHICE, excursions II and III, and the EAREZE (or excursion IV). The
- lack of statistically significant covariance between $\delta^{13}C_{carb}$ and $\delta^{18}O_{carb}$ (R \approx 0.012; Fig. S2), is
- not in itself definitive evidence of preservation, but it is consistent with only limited diagenetic
- influence on the δ^{13} C_{carb} record (Kaufman and Knoll, 1995). Whereas δ^{18} O_{carb} values are low (–
- 366 12% to -2%), this depletion likely reflects post-depositional fluid interaction, as $\delta^{18}O_{carb}$ is
- more sensitive to alteration than δ^{13} C, which often retains its original marine signal (Banner and
- 368 <u>Hanson, 1990</u>). Although post-depositional alteration is evident in the oxygen isotope record,
- the long-term $\delta^{13}C_{carb}$ pattern remains consistent with primary marine signals and is therefore
- suitable for high-resolution chemostratigraphic correlation (Álvaro et al., 2008; Jamart et al.,
- 371 <u>2025</u>).
- 372 The following carbon isotope descriptions are based on the 35-point moving average general
- 373 trend observed in the $\delta^{13}C_{carb}$ data.
- 374 The $\delta^{13}C_{carb}$ curve recorded in Tiout closely matches the composite curves of Maloof et al.
- 375 (2010) for other sections in the western Anti-Atlas of Morocco. Their curves were used in the

- 376 GTS 2020 volume (Cramer and Jarvis, 2020; Peng et al., 2020) to reconstruct the global
- carbon isotope excursion framework of the Cambrian in terms of excursion morphology,
- magnitude, and stratigraphic position. At the base of the section (0 to \sim 70 m) within the lower
- Lie de vin Formation, $\delta^{13}C_{carb}$ values start near -4% and define a sustained negative value that
- is interpreted as the termination of the SHICE. First described from the Chiungchussu
- Formation in eastern Yunnan, South China platform (Zhu et al., 2006a), the negative SHICE is
- a (sub)globally traceable carbon cycle perturbation recorded in Cambrian Stage 2. Zhu et al.
- 383 (2006b) associated the SHICE with an extinction of SSFs in South China, that is also
- documented in North Gondwana (South Australia, (Betts et al., 2018)), Although the SHICE
- should be seen as a low diversity interval with persistence of a number of earlier appearing
- fossil genera and species, coeval strata in East Siberia and the Avalonia do not show a loss in
- diversity or faunal turnover in SSF communities that appeared with the onset of the older,
- 388 strongly positive ZHUCE excursion (Landing and Kouchinsky, 2016; Kouchinsky et al.,
- 389 <u>2017; fig. 5</u>).
- The fall of the SHICE to negative values marks the transition from the positive Zhujiaqing
- 391 Carbon Isotope Excursion (ZHUCE) to more stable isotopic values in upper Terreneuvian
- strata. SHICE values typically range from -4% to -6%, reaching as low as -9% in South
- 393 China (Zhu et al., 2006a), and have been identified in Siberia ("6n"; Kouchinsky et al. (2007),
- South Australia (Betts et al., 2018) and in the nearby Oued Sdas section of the Moroccan
- 395 Anti-Atlas (Maloof et al., 2010).
- 396 At Tiout, the SHICE is temporally constrained by several undated volcanic ash beds near
- 397 ~88.5 m, which are stratigraphically consistent with ash bed M234 from the Oued Sdas
- section (dated at 523.17 ± 0.16 Ma; Maloof et al., 2010), providing a chronostratigraphic
- anchor for the lower part of the section.
- 400 Following the SHICE, two minor $\delta^{13}C_{carb}$ peaks occur: the lower one at ~ -1.5% around 300
- 401 m, and a second at \sim -3% around 450 m (Fig. 3). These are interpreted as excursions II and
- 402 III, respectively, originally recorded in lower Cambrian strata on the Siberian Platform
- 403 (Magaritz et al., 1986; Kirschvink et al., 1991). On the Siberian platform, both excursions fall
- 404 within the *Dokidocyathus regularis* Zone of the regional middle Tommotian Stage
- 405 (<u>Kouchinsky et al., 2007</u>; <u>Kouchinsky et al., 2015</u>).
- 406 From that level, $\delta^{13}C_{carb}$ values decrease gradually upsection at Tiout, reaching to a broad
- 407 negative excursion that bottoms out at -4% at ~600 m. This represents the most depleted
- 408 interval in the section and aligns stratigraphically with ash bed Ti 566, dated at 521.06 ± 0.12
- 409 Ma (Landing et al., 2021b).

Between ~ 600 m and ~ 1150 m, the $\delta^{13}C_{carb}$ curve displays a broad, symmetric positive 410 excursion, corresponding to the EAREZE (Fig. 3). The EAREZE positive excursion has been 411 recognized in several regions, including the Siberian Platform (Magaritz et al., 1986; Brasier 412 et al., 1994; Derry et al., 1994; e.g., Kouchinsky et al., 2007), Morocco (Maloof et al., 2010), 413 and northwesternmost Canada (Dilliard et al., 2007). However, the positive excursion in 414 415 Australia ((peak II in Betts et al. (2018); CARE in Betts et al. (2024)) and South China (Yang 416 et al., 2025) likely represents the slightly younger CARE peak (e.g., Geyer, 2019a). The 417 δ¹³C_{carb} values for the EAREZE range from approximately +1.4‰ in Siberia to +3.4‰ in the 418 Moroccan sections. 419 The EAREZE, as well as the CARE (believed in some reports to be coeval), were considered to align roughly with the initial radiation of trilobites and diverse arthropods (Brasier et al., 420 1994; Zhu et al., 2006a; Bowyer et al., 2022) and to be more-or-less coeval with the LO of 421 trilobites in a number of regions (Zhu et al., 2006a). However, the CARE isotope event in 422 South China corresponds with the *Parabadiella huoi* Zone for which a radiometric date of ca. 423 518 Myr has been recorded (Yang et al., 2018; Fu et al., 2019). High precision dating in the 424 Tiout section prove an age of >519.5 Myr (Landing et al., 2021b) for the EAREZE peak. 425 426 Stratigraphically, the EAREZE peak lies several trilobite biozones below the *Choubertella* 427 Zone. Since the Choubertella Zone is thought to correlate with the Parabadiella huoi Zone of South China (Geyer, 2019a), this indicates that the EAREZE peak predates the interval of the 428 429 CARE event. On the Siberian Platform, the EAREZE peak lies in the *Repinaella* Zone, above the base of the regional Atdabanian Stage (Geyer, 2019a), with its base marked by the LO of 430 431 Profallotaspis jakutensis, approximately in the lowest part of excursion IV (e.g., Varlamov et al., 2008). 432 In this study, the LO of identifiable trilobites at Tiout and in West Gondwana is recorded at 433 ~1048.3 m on the declining limb of the EAREZE excursion, based on *in situ* field indicators 434 435 "T" identified by Sdzuy (1978) and confirmed by Geyer (2019c). Similarly old trilobite assemblages with a comparable composition are known from the Pedroche and Alconera 436 formations of southern Spain (Liñán et al., 2005; Liñán et al., 2008), but the relevant sections 437 appear to be unsuitable for revealing carbon isotope signatures. In Tiout, the EAREZE peaks 438 439 at +2%, corresponding to ~910 m within the lower Igoudine Formation. The EAREZE is bracketed by two dated volcanic ash beds: Ti 566 at its base and Ti-Am.0.0 at 1137.7 m (dated 440 at 519.23 ± 0.14 Ma, Landing et al. (2021b). 441

3.3. Identification of astronomical forcing in detrital proxies

442

To investigate astronomical forcing recorded in the Tiout section, we selected SiO₂, TiO₂, and 444 Al₂O₃ as geochemical proxies (Figs. 3–5). These chemicals are well-established indicators of 445 terrigenous input in mixed carbonate-siliciclastic systems (Calvert and Pedersen, 2007) and 446 447 are commonly used in deep-time paleoclimate reconstructions (Li et al., 2019; Sinnesael et al., 2019; Arts et al., 2024; Pas et al., 2024). Elevated concentrations of these detrital proxies in 448 marine sediments is typically associated with increased runoff, likely linked to intensified 449 precipitation or sea-level fall (e.g., Da Silva et al., 2013; Pas et al., 2018). However, the 450 expression of detrital input may vary depending on the temporal resolution and depositional 451 452 context. Among these elements, SiO₂ was chosen as the reference proxy for time series analysis due to its high variability in our record, pronounced sensitivity to climatic variations 453 454 (Calvert and Pedersen, 2007) and strong correlation with other detrital proxies (Fig. 3), which 455 also indicate minimal diagenetic alteration. 456 As documented in previous studies (Monninger, 1979; Sinnesael et al., 2024), the lower Cambrian Stage 2 strata of the Tiout section are marked by striking rhythmic alternations 457 458 between lighter-colored marlstones and darker limestones, which is particularly well 459 expressed in the Lie de vin Formation (Fig. 4). These rhythmic patterns occur across several 460 scales of bundled cyclicity: meter-scale alternation "rhythms", decameter-scale "cyclothems" composed of several rhythms, 100 m-scale sequences "supercycles," and long-term trends 461 spanning several hundred to over a thousand meters. The bundling of meter-scale depositional 462 rhythms into higher-order cyclothems, expressed in the Tiout section weathering profile, has 463 been interpreted as the sedimentary manifestation of paleoclimate changes driven by 464 precession and short-eccentricity cycles (Sinnesael et al., 2024). This interpretation is 465 supported by independent high-precision U-Pb zircon CA-ID-TIMS ages from multiple 466 bentonite layers throughout the stratigraphic interval. 467 To evaluate the imprint of orbital forcing on the detrital proxy record at the cyclothem scale 468 (20-40 m), we compared the weathering profile captured in drone imagery with the highly 469 resolved SiO₂ stratigraphic profile. As illustrated in Fig. 4, elevated SiO₂ concentrations 470 471 consistently coincide with marlstone-rich intervals, indicating that detrital input faithfully tracks lithological alternations at this scale. This supports the use of SiO₂ as a robust proxy for 472 473 time-series analysis throughout the Tiout section. In this study, all published bentonite-based ages were located with a resolution of 1.5 m in the succession. Using the thickness of the 474 section and the time interval constrained by numerical ages at its base and top, we estimate an 475 average sediment accumulation rate of 260 m/Myr, which is consistent with values in other 476 477 reports (Landing et al., 2021b; Sinnesael et al., 2024).

To account for changes in sedimentation rate as observed in previous studies, we assume that 478 479 the short eccentricity cycle is expressed with a wavelength ranging from 20 to 40 m. Based on 480 this range, the corresponding expected wavelength would be approximately ~74–147 m for the long eccentricity (405 kyr), \sim 5.8–11.6 m for obliquity (\sim 32 kyr), and \sim 3.3–6.7 m for 481 precession (~18.3 kyr). These estimates are based on the predicted early Cambrian 482 483 astronomical frequency ratios (22.13:3.6:1) (Laskar et al., 2004; Waltham, 2015; Farhat et al., 484 <u>2022</u>). The CWT of the log₁₀-transformed SiO₂ series (Fig. 5A) reveals prominent spectral powers at 485 486 wavelength bands interpreted as the ~110 kyr short eccentricity cycle, as well as the expected 487 obliquity and a precession cycles. Weaker spectral power is also observed at the ~405 kyr long eccentricity cycle. Due to the 1.5-m sampling resolution, our confidence in interpreting 488 489 cycles thinner than ~6 m is limited (Martinez et al., 2016), and the 5.5 m peak lies at the lower threshold of reliable detection. The precession–eccentricity origin for the Tiout sedimentary 490 record was assessed by filtering out the 5.5 m periodicity and applying spectral analysis on its 491 492 Hilbert transform envelope (Fig. S3). The power spectrum shows one main amplitude modulation frequency at 0.035 cycles/cm (28 m), which indicate a modulation of m-scale 493 494 cyclicity by decameter-scale cycle (i.e., "cyclothem" of this report). 495 3.4. Astronomical calibration for the Tiout section 496 497 Assuming that Milankovitch forcing governs the multi-scale cyclicity in the Tiout section and given the particularly well-expressed short eccentricity component in the stratigraphic record, 498 we applied a Taner bandpass filter targeting the 20-40 m wavelength range. Assuming a short-499 eccentricity cycle of ~110 kyr we constructed a floating astronomical timescale spanning 4.87 500 \pm 0.11 Myr for the Tiout section (Fig. 5B). The CWT of the astronomically calibrated SiO₂ 501 series (Fig. 5B) reveals distinct power in the 1.2 Myr, 405 kyr, ~110 kyr (calibrated) and ~32 502 503 kyr range, and a weaker but high non-negligible power in the band of 173 kyr obliquity, precession cycles (~18.2 kyr), and a ~55 kyr, which correspond to a secondary obliquity-504 505 related component in today's time (<u>Laskar</u>, 2020), but whether an analogous component operated in the Cambrian is unknown. The periodicity of power peaks in the CWT scalogram 506 507 of the tuned SiO₂ series aligns with the expected early Cambrian duration (Laskar et al., 2004; Waltham, 2015; Farhat et al., 2022; Wu et al., 2024), which supports our astronomical 508 509 interpretation. Band-pass filters for wavelength bands of $20-40 \text{ m} (0.025-0.05 \text{ m}^{-1})$ and $70-130 \text{ m} (0.0077-0.05 \text{ m}^{-1})$ 510

0.0143 m⁻¹) representing short and long eccentricity (~405 kyr) are also shown in Fig. 5B. The

short eccentricity (~110 kyr) filter and its Hilbert transform envelope shows amplitude modulation that is mostly in antiphase with the 405 kyr filter, which supports an astronomical forcing for the observed cyclicity. This antiphase relationship, further detailed in Fig S4, likely indicates the processes that drive the proxy record (e.g. SiO₂) respond in the opposite direction than the astronomical forcing. Modulation of precession is further confirmed by spectral analysis of the precession-filter envelope, which reveals a robust ~110 kyr amplitude modulation (Fig. S4).

The short-eccentricity cycle (~110 kyr) is the most visually striking and laterally consistent cyclicity present in the Tiout section. Based on lithological and geochemical observations, darker intervals (dominated by carbonate-rich facies) alternate with lighter-colored, detrital-rich intervals. We interpret these alternations as the climatic response to eccentricity pacing: eccentricity maxima, associated with intensified monsoon will drive enhanced water circulation and nutrient supply allowing thrombolite to thrive (e.g., higher carbonate productivity). Minima will promote lower carbonate productivity under less stable, open marine conditions.

While our interpretation differs in its underlying mechanism, it corresponds closely in the observed stratigraphic expression to the cyclothem framework established by Monninger (1979), which identified a recurring ~30 m-thick facies cycle based on patterns in lithology, bed thickness, and the relative abundance of carbonate and detrital units. Monninger (1979) documented that stromatolitic-thrombolite bioherms tend to peak near the center of these cycles, with variations in size and abundance reflecting transitions from more restricted to more open marine conditions. We suggest that these environmental gradients were likely controlled by orbital eccentricity. In this context, short eccentricity maxima, associated with enhanced water circulation and open marine conditions, likely promoted increased water circulation, providing more nutrient and more stable marine conditions that enhanced stromatolite growth and carbonate accumulation (Andres and Reid, 2006) and resulted in well-developed bioherms near the center of each cycle. In contrast, eccentricity minima decrease water circulation and possible restriction or turbidity, conditions less favorable for algal colonization and carbonate precipitation. Thus, the ecological and sedimentological patterns documented in Monninger (1979) are consistent with a climatic control paced by eccentricity forcing, with nutrient and water circulation effects dominate carbonate sedimentation and thrombolites developments. This integrated view reconciles nonlinear sedimentary and ecological responses to astronomically paced environmental change.

547 3.5. Bayesian astrochronology: new age constraints for early Cambrian events The Bayesian age-depth model integrates high-precision CA-ID-TIMS U-Pb zircon ages 548 (Maloof et al., 2010; Landing et al., 2021b) with stratigraphic tie-points derived from well-549 expressed 20–40 m-thick cycles, interpreted to record ~110 kyr short eccentricity (Fig. 5). 550 The peak of the EAREZE is now dated at 520.046 +0.097/-0.095 Ma (95% HPD) by this 551 report, which is the most precise numerical age constraint for this carbon isotope excursion to 552 date. While Landing et al. (2021b) estimated the peak of the EAREZE in the Anti-Atlas of 553 554 Morocco at 520.27 +0.59/-0.57 Ma through interpolation between radiometrically dated tuffs and by assuming uniform sediment accumulation rates, the new high-resolution $\delta^{13}C_{carb}$ data 555 556 presented here allow for a more precise stratigraphic location of the EAREZE peak within the 557 Tiout section. By precisely locating the excursion in a well documented succession and 558 integrating it with existing U-Pb geochronology and astrochronological data from the same section, our model reduces previous uncertainty estimates by nearly an order of magnitude. 559 560 In addition, the lowest known occurrence (LO) of fragmentary and unidentifiable mineralized 561 trilobites near the base of the lower member of the Igoudine Formation lies near the peak of 562 EAREZE and is constrained to 519.62 +0.11/-0.11 Ma (95% HPD). 563 This places the lowest known Moroccan trilobite fragments as an approximate correlative of lower Repinaella Zone trilobites in east Siberia (Varlamov et al., 2008). Simultaneously, the 564 LO of identifiable trilobites in West Gondwana, marked by the appearance of the Hupetina 565 antiqua faunule in the Tiout Member (Geyer, 2019b) is now constrained to 519.494 +0.117/-566 0.113 Ma (95% HPD), defining a ~552 kyr lag between this facies-controlled appearance 567 nearly at the lithofacies transition from massive carbonates of the lower member of the 568 Igoudine and the Tiout Member event and the peak of the EAREZE. 569 The new LO age for the trilobite fragments is equivalent than the estimate from model A in 570 Sinnesael et al. (2024) (519.70–519.54 Ma, 95% HPD) and ~330 kyr younger than the 571 interpolated estimate of 519.95 +0.43/-0.40 Ma defined in Landing et al. (2021b), while still 572 573 overlapping within uncertainty bounds. 574 In addition to calibrating the date on EAREZE and the lowest fragmentary trilobite remains 575 and the date on the LO of the lowest identifiable trilobites, this model yields updated ages for 576 other key early Cambrian δ^{13} C excursions and a new age for the LO of archaeocyaths (Fig. 6). 577 Excursion II is now constrained to 522.413 +0.071/-0.070 Ma and excursion III to 521.724 578

+0.065/-0.065 Ma, while the LO of archaeocyaths yield an age of 519.44 +0.117/-0.113 Ma, all expressed with 95% HPD. All Baysian ages model results are summarized in Table 1.

581 582

3.6. Implications for the timing of early Cambrian biogeochemical events in West Gondwana

583 584

These new ages estimate the lowest occurrences of mineralized trilobite fragments and the 585 younger occurrence of identifiable trilobites and align with other global datasets, but with 586 587 significantly reduced uncertainty (Fig. 6). A dated ash bed in the Caerfai Bay Shales 588 Formation of Pembrokeshire, Wales, eastern Avalonia, located just above the LO of trilobites 589 was dated at 519.30 ± 0.23 Ma (Landing et al., 1998; Harvey et al., 2011; Landing et al., 590 2013b). However, the trilobites on the Avalonia continent are locally known to be very late 591 arrivals, with the oldest trilobites in the Brigus Formation of western Avalonia far younger and dating to somewhat older than ca. 507.91 ± 0.07 Ma. These dates demonstrate the very 592 593 diachronous LO of trilobites (Landing et al., 2023). In South China, Zhang et al. (2022a) 594 estimated the LO of trilobites at 520.11 ± 1.91 Ma, anchoring a floating astrochronology to a 595 low-precision SHRIMP U-Pb date. In both cases, uncertainties exceed 460 kyr to nearly 4 Myr. In other sections worldwide, the precise timing of the trilobite LO remains indirectly 596 constrained (i.e., absence of direct age control) and is inferred from its stratigraphic position 597 relative to the EAREZE and CARE. No radiometric dates exist for the oldest strata with 598 trilobites on the Baltica paleocontinent. This Schmidtiellus mickwitzi fauna in Estonia has 599 600 been equated with the Skiagia ornata-Fimbriaglomerella membranacea acritarch assemblage (Moczydłowska, 1998; Schoenemann et al., 2017) and was considered as particularly old. 601 However, the acritarch assemblage appears to be controlled by facies rather than indicating a 602 603 robust age, and several data suggest a much younger age of these oldest trilobites of Baltica 604 (Geyer and Landing, 2018; Geyer, 2019c). In Siberia, trilobites such as *Profallotaspis jakutensis* occur below the EAREZE peak (at the 605 606 onset of EARZEE) at the base of the Atdabanian Stage (Kirschvink et al., 1991; Kouchinsky et al., 2007; Rozanov et al., 2008; Bowyer et al., 2022). Similar stratigraphic relationships 607 have been described for the Tarim Platform (Yang et al., 2025), and Laurentian northwestern 608 Canada (Dilliard et al., 2007). However, the δ^{13} C excursions in these regions need to be 609 examined in their relationship to precise biostratigraphical data. In South Australia (Betts et 610 611 al., 2018), the oldest trilobite assemblage includes *Parabadiella huoi* and thus appears to be 612 coeval with the onset of the trilobites in South China (Geyer, 2019). An SSF assemblage with

Micrina etheridgei slightly predates the P. huoi Biozone on the lower limb of the CARE 613 614 positive excursion. The oldest identified Laurentian trilobites are known from well studied sections in the Great 615 616 Basin (southern Nevada and California) originally claimed to represent a Fallotaspis fauna similar to the oldest known trilobites of Morocco (e.g., Hollingsworth, 2005a; Hollingsworth, 617 2005b; Hollingsworth, 2007). Revised identifications suggest the oldest identified trilobites to 618 619 represent a relatively endemic fauna dominated by archaeaspidids (Fritzaspis Zone) and 620 subsequent fallotaspidids (e.g., Hollingsworth, 2011). Unfortunately, these fossiliferous sections from the Great Basin are dominated by siliciclastics and are unlikely to provide 621 carbon isotope signatures. Records of $\delta^{13}C$ fluctuations are known from the Sekwi Mountains 622 of the Canadian Cordillera and indicate a distinct positive shift in the "Fallotaspis Zone" 623 (Dilliard et al., 2007). However, the fossil record in the relevant sections is sparse (Fritz, 624 625 1976) and does not allow a precise correlation with the Great Basin sections. In contrast, in the Moroccan sections such as Tiout and Oued Sdas, the LO of the lowest 626 627 known trilobite fragments and identifiable trilobites lies above or on the declining limb of the EAREZE excursion (this study; Tucker, 1986; Maloof et al., 2010; Geyer, 2019c). 628 629 The apparent broad global inconsistency in the stratigraphic position of trilobite LOs relative 630 to the positive carbon isotope excursions means that careful consideration must be given to interregional correlations, which require a combination of δ^{13} C frameworks and inferred tie-631 632 points, precise radiometric dating, and biostratigraphic data. The Bayesian age modeling presented herein overcomes these limitations by anchoring the EAREZE within an integrated 633 634 geochronologic and cyclostratigraphic constrained sequence providing a more robust temporal calibration. 635 636 637 3.7. Evaluation of the EAREZE (Excursion IV) as a global chronostratigraphic marker 638 Efforts to define a globally synchronous base for Cambrian Series 2 have been hindered by the diachronous nature of the trilobite first appearance datums, which vary regionally in both 639 their absolute timing and taxonomic composition (Geyer and Shergold, 2000; Peng et al., 640 2012; Landing et al., 2013a; Zhu et al., 2019; Landing et al., 2024). Regional index fossils 641 have been used to approximate the base of Cambrian Series 2, but none satisfies the key 642 criteria for a GSSP of broad geographic distribution, consistent preservation, and near-643 synchronous definition between diverse paleoenvironments. Their utility is further limited by 644 pronounced endemism, strong biofacies and taphonomic biases: these trilobites are typically 645 restricted to inner-shelf siliciclastic settings and are rarely preserved or recoverable as 646

identifiable specimens in carbonate-dominated or deeper-water successions, limiting global 647 648 correlation. In Morocco's continuous successions, this facies dependence likely explains the relatively young LO of identifiable trilobites, which is corroborated by undetermined trilobite 649 remains lower in the Igoudine Formation (Sdzuy and Geyer, 1988). Such issues undermine 650 the reliability of trilobite LOs as reliable global stratigraphic tie-lines, particularly in the lower 651 Cambrian strata dominated by high provincialism (Landing et al., 2013a). As a result, 652 attention has increasingly shifted toward geochemical markers, in particular carbon isotope 653 excursions, as potential chronostratigraphic anchors. Among these, the EAREZE positive 654 655 δ¹³C_{carb} excursion has emerged as a leading candidate to help bracket the base of Cambrian Series 2. Its widespread stratigraphic expression on different paleocontinents (e.g., West 656 657 Gondwana, Siberia, Avalonia, and Laurentia) below the CARE positive δ^{13} C_{carb} excursion of 658 the South China and North China paleocontinents as well as Australia means that CARE can 659 be used as an auxiliary marker. The temporal association of EAREZE with the later part of the early skeletal metazoan radiation, including trilobites and archaeocyaths (Kirschvink et al., 660 661 1991; Zhu et al., 2006a; Kouchinsky et al., 2007; Maloof et al., 2010; Kouchinsky et al., 2012; Betts et al., 2018), highlights its importance (Fig. 7). Where both chemostratigraphic 662 663 and biostratigraphic records are available, the LOs of identifiable mineralized trilobites generally occur in close stratigraphic proximity to the EAREZE peak: below in Siberia 664 (Profallotaspis Zone), and apparently in the Sekwi Mountains of Laurentian northwestern 665 Canada (i.e., earlier reported "Fallotaspis" interval) (Kirschvink et al., 1991; Zhu et al., 666 2006a; Dilliard et al., 2007; Kouchinsky et al., 2007; Rozanov et al., 2008; Betts et al., 2018; 667 Bowyer et al., 2023; Yang et al., 2025). In the Tiout section, the lowest determinable trilobites 668 were collected above the EAREZE peak, but probably within the trilobite range as indicated 669 670 by small, undeterminable sclerite fragments. This temporally constrained coupling of biological and geochemical signals highlights the 671 diagnostic utility of the EAREZE. It offers a chemostratigraphic framework against which 672 diachronous trilobite appearances can be compared and calibrated. Its reproducibility, 673 674 independence from facies control, and association with major biogeochemical reorganization including increased carbonate platform development, possible redox shifts, and enhanced 675 676 organic carbon burial, support its interpretation as a first-order perturbation in the early Cambrian (Brasier et al., 1994; Derry et al., 1994; Zhu et al., 2006a; Wood and Erwin, 2018; 677 Alexander et al., 2025). 678 To sum up, the EAREZE (IV) excursion satisfies key requirements for consideration as part of 679 680 the definition of a GSSP-level marker. It exhibits (1) wide geographic expression across

multiple paleocontinents; (2) a clear and reproducible geochemical signature; (3) independent 681 682 confirmation across multiple stratigraphic datasets; and (4) a close temporal association with globally significant biotic transitions. The Tiout section, in particular, meets several additional 683 684 criteria outlined for GSSP candidates: It is highly accessible, features an expanded and continuous sedimentary record and shows preservation with minimal tectonic deformation. 685 Moreover, the precise age calibration of both the EAREZE and the LOs of fragmentary, 686 unidentified and higher identifiable trilobites at Tiout provides a critical temporal anchor for 687 688 synchronizing lower Cambrian successions globally. 689 The EAREZE is a strong candidate for bracketing the base of Cambrian Series 2 and for refining the chronology of the Cambrian Explosion. However, a GSSP of a geochronologic unit is a 690 691 "golden spike" that defines a specific horizon and point at the unit's type section, while the 692 onset, peak, and fall of EAREZE brackets a significant stratigraphic interval at Tiout (Fig. 3). 693 To resolve the ambiguity of the use of EAREZE/CARE in definition of a Series 2 and Stage 3 basal GSSP, Landing et al. (2013a) proposed the use of the peak of EAREZE (which they 694 695 termed "CARE") for interregional correlation and, specifically, the appearance of *Repinaella* at the Zhurinsky Mys section on the Lena River on the Siberian Platform (e.g., Varlamov et al., 696 2008) to define the base of Series 2 and Stage 3. 697

698 699

700

4. CONCLUSIONS

Resolving the global tempo and drivers of early Cambrian biological and geochemical 701 702 changes requires stratigraphic sections that combine fossiliferous data, precise dating, and 703 well-preserved environmental signals. The Tiout section in the western Anti-Atlas of Morocco meets these criteria. Through integration of our new $\delta^{13}C_{carb}$ data, biostratigraphy, high-704 precision CA-ID-TIMS U-Pb zircon dating, pXRF-based detrital proxies, and 705 706 astrochronology, we present a comprehensive high-resolution chronostratigraphic framework 707 for the late Terreneuvian-early Cambrian Series 2 interval. 708 Time series analysis of pXRF-derived log-SiO₂ and other detrital proxies reveals prominent 709 cyclicities corresponding to Milankovitch-scale orbital forcing, including short eccentricity 710 and precession. These results align with a previously suggested astronomical origin of the observed meter- to decameter-scale stratigraphic bundling and justify the construction of a 711 712 floating astronomical time scale for the Tiout section that brackets a 4.87 ± 0.11 Myr interval. Building on our astronomical interpretation, we constructed a Bayesian age-depth model that 713 714 integrates all available geochronological and paleontological data points, and major

geochemical events. This model constrains the peak of the EAREZE (excursion IV) to 715 520.046 +0.097/-0.095 Ma (95% HPD), provides the first direct numerical quantification of 716 717 this geochemical event within a single stratigraphic framework, and embeds it in a global time 718 scale. 719 The LO of identifiable trilobites in West Gondwana, recorded at Tiout by the onset of the Hupetina antiqua assemblage, is dated to 519.494 +0.117/-0.113 Ma, defining a ~552 kyr lag 720 between the peak of the EAREZE and this LO event. Additionally, the Tiout age model also 721 provides the first age estimate for the early Cambrian δ^{13} C_{carb} excursions II and III, at 522.413 722 723 +0.071/-0.07 Ma and 521.724 +0.065/-0.065 Ma, each with 95% HPD intervals of $\sim 130-140$ 724 725 The 552 kyr temporal decoupling between the onset of the EAREZE and the LO of identified 726 is consistent with globally observed patterns: in regions such as on the Siberian Platform and 727 Laurentian Canada, the LO of mineralized and identifiable trilobites lies slightly below the EAREZE peak, whereas the lowest determinable trilobites in the Moroccan Atlas ranges were 728 729 collected above the peak (although the true onset in the Anti-Atlas appears to be lower). The 730 slightly younger CARE first defined in South China Platform and reported on the Tarim 731 Platform and in South Australia lies approximately at the LO of mineralized trilobites in these 732 regions. These results enable the worldwide LOs of trilobites in the early Cambrian to be calibrated when stratigraphically associated with the EAREZE and CARE excursions. 733 The EAREZE meets key criteria for contributing to a GSSP-level marker for the base of 734 Series 2 and Stage 3: (1) broad geographic distribution; (2) replicability; (3) high-resolution 735 temporal constraint; and (4) strong evolutionary relevance. As such, the EAREZE is important 736 for defining the base of Cambrian Series 2. However, the position of a global GSSP has to be 737 738 defined within the range of EAREZE, with one multiproxy stratum suggested at the peak of 739 EAREZE approximately at the LO of the trilobite Repinaella in eastern Siberia or a 740 comparable useful candidate elsewhere. The idea of the use of a "FAD of trilobites" to define the base of Series 2 (e.g., Zhu et al., 2019) is not appropriate as the early diversification of 741 742 trilobites was likely in the much older Terreneuvian and involved poorly/weakly mineralized 743 taxa (Paterson et al., 2019) with mineralization controlled by the transition from an aragonitic 744 to a calcitic ocean (Porter, 2007; Landing et al., 2024). Altogether, the Tiout section provides a temporally resolved, stratigraphically continuous, and 745 geochemically calibrated reference for the early Cambrian. It significantly advances global 746 correlation and stage boundary definition efforts by embedding fossil and new $\delta^{13}C_{carb}$ data 747 748 within a high-resolution temporal framework. The Tiout model reinforces the EAREZE as a

- 749 primary chronostratigraphic anchor for the base of Cambrian Series 2 and contributes critical
- 750 clarity to the tempo and structure of early animal radiation and Earth system reorganization.
- 752 **5. Acknowledgements**

758

762

765

767

- D.P. and V.J. are funded by an SNF Ambizione Grant (n°193520). A.C.D.S and J.J.C.H.
- thanks the FNRS grants (T.0037.22). K. M., J.O., M.A.B. and N.Y. were supported by the
- 755 Cadi Ayyad University, the Faculty of Sciences-Semlalia and the Hassan II Academy of
- Science and Technology grant (led by N.Y.). Field and laboratory work by E.L. and G.G. was
- done under U.S. National Science Foundation grants.
- 759 **6. Supplementary**
- Supplementary Materials 1 Geochemical dataset: Contains all the pXRF-derived proxies,
- 761 $\delta^{13}C_{carb}$, $\delta^{18}O_{carb}$, lithological and key marker beds position.
- Supplementary Materials 2 Times series analysis scripts, full model priors, OxCal code, and
- 764 posterior outputs.
- 766 Supplementary Materials 3 Supplementary figures 1-5.
- 768 7. Reference list
- Alexander, R.D., Zhuravlev, A.Y., Bowyer, F.T., Pichevin, L., Poulton, S.W., Kouchinsky, A. and Wood, R., 2025. Low oxygen but dynamic marine redox conditions permitted the Cambrian Radiation. Science Advances, 11(4): eads2846, https://doi.org/10.1126/sciadv.ads2846
- Álvaro, J.J., Bauluz, B., Subias, I., Pierre, C. and Vizcaïno, D., 2008. Carbon
 chemostratigraphy of the Cambrian-Ordovician transition in a midlatitude mixed
 platform, Montagne Noire, France. Geological Society of America Bulletin, 120(7-8):
 962-975, https://doi.org/10.1130/B26243.1
- Andres, M.S. and Reid, P.R., 2006. Growth morphologies of modern marine stromatolites: A case study from Highborne Cay, Bahamas. Sediment. Geol., 185(3): 319-328, https://doi.org/10.1016/j.sedgeo.2005.12.020
- 781 Arts, M., 2023. WaverideR: Extracting Signals from Wavelet Spectra. https://cran.r-project.org/package=WaverideR.
- Arts, M., Corradini, C., Pondrelli, M., Pas, D. and Da Silva, A.-C., 2024. Age and orbital forcing in the upper Silurian Cellon section (Carnic Alps, Austria) uncovered using the WaverideR R package. Frontiers in Earth Science, 12,
- 786 https://doi.org/10.3389/feart.2024.1357751

- Aubry, M.-P., 2015. Biostratigraphy. In: W.J. Rink and J.W. Thompson (Editors), Encyclopedia of Scientific Dating Methods. Springer Netherlands, Dordrecht, pp. 83-107, https://doi.org/10.1007/978-94-007-6304-3 192
- Banner, J.L. and Hanson, G.N., 1990. Calculation of simultaneous isotopic and trace element
 variations during water-rock interaction with applications to carbonate diagenesis.
 Geochemica & Cosmochimica Acta, 54: 3123-3137
- Betts, M.J., Claybourn, T.M., Holmer, L.E., Skovsted, C.B., Myrow, P.M., Stemmerik, L.,
 Topper, T.P., Park, T.-Y.S., Hughes, N.C., Crowley, J.L., Jagodzinski, E.A. and Brock,
 G.A., 2024. First multi-proxy chronostratigraphy of the lower Cambrian Byrd Group,
 Transantarctic Mountains and correlation within East Gondwana. Gondwana Res.,
 136: 126-141, https://doi.org/10.1016/j.gr.2024.07.022
 - Betts, M.J., Paterson, J.R., Jacquet, S.M., Andrew, A.S., Hall, P.A., Jago, J.B., Jagodzinski, E.A., Preiss, W.V., Crowley, J.L., Birch, S.A., Mathewson, C.P., García-Bellido, D.C., Topper, T.P., Skovsted, C.B. and Brock, G.A., 2018. Early Cambrian chronostratigraphy and geochronology of South Australia. Earth Sci. Rev., 185: 498-543, https://doi.org/10.1016/j.earscirev.2018.06.005

800

801 802

805 806

807

808

809

810 811

812

813

814 815

816

817

818

819

820 821

822

823

824

- Bottjer, D.J., Hagadorn, J.W. and Dornbos, S.Q., 2000. The Cambrian substrate revolution.

 GSA today, 10(9): 1-7
 - Bowring, S.A., Grotzinger, J.P., Isachsen, C.E., Knoll, A.H., Pelechaty, S.M. and Kolosov, P., 1993. Calibrating rates of early Cambrian evolution. Science, 261(5126): 1293, https://doi.org/10.1126/science.11539488
 - Bowyer, F.T., Zhuravlev, A.Y., Wood, R., Shields, G.A., Zhou, Y., Curtis, A., Poulton, S.W., Condon, D.J., Yang, C. and Zhu, M., 2022. Calibrating the temporal and spatial dynamics of the Ediacaran Cambrian radiation of animals. Earth Sci. Rev., 225: 103913, https://doi.org/10.1016/j.earscirev.2021.103913
 - Bowyer, F.T., Zhuravlev, A.Y., Wood, R., Zhao, F., Sukhov, S.S., Alexander, R.D., Poulton, S.W. and Zhu, M., 2023. Implications of an integrated late Ediacaran to early Cambrian stratigraphy of the Siberian Platform, Russia. GSA Bulletin, 135(9-10): 2428-2450, https://doi.org/10.1130/b36534.1
 - Brasier, M.D., Anderson, M.M. and Corfield, R.M., 1992. Oxygen and carbon isotope stratigraphy of early Cambrian carbonates in southeastern Newfoundland and England. Geol. Mag., 129(3): 265-279, 10.1017/S001675680001921X
 - Brasier, M.D., Corfield, R.M., Derry, L.A., Rozanov, A.Y. and Zhuravlev, A.Y., 1994. Multiple δ13C excursions spanning the Cambrian explosion to the Botomian crisis in Siberia. Geology, 22(5): 455-458, <a href="https://doi.org/10.1130/0091-7613(1994)022<0455:MCESTC>2.3.CO;2">https://doi.org/10.1130/0091-7613(1994)022<0455:MCESTC>2.3.CO;2
 - Brasier, M.D. and Cowie, J.W., 1989. Other areas: North-west Canada; California, Nevada, and Mexico; Morocco, Spain, and France. In: J.W. Cowie and M.D. Brasier (Editors), The Precambrian-Cambrian Boundary. Oxford Monograph on Geology and Geophysics, 12. Clarendon Press, Oxford, 105-114
- Brasier, M.D. and Sukhov, S.S., 1998. The falling amplitude of carbon isotopic oscillations through the Lower to Middle Cambrian: northern Siberia data. Canadian Journal of Earth Sciences, 35(4): 353-373, 10.1139/e97-122
- Calvert, S.E. and Pedersen, T.F., 2007. Chapter Fourteen Elemental Proxies for Palaeoclimatic and Palaeoceanographic Variability in Marine Sediments: Interpretation and Application. Developments in Marine Geology, 1: 567-644, https://doi.org/10.1016/S1572-5480(07)01019-6
- Castle-Jones, J., Betts, M.J., Holmes, J.D., Klaebe, R.M., Hall, P.A., Crowley, J.L., Zhang, Z.L. and Brock, G.A., 2025a. Integrated biostratigraphy, chemostratigraphy and geochronology of the lower Cambrian succession in the western Stansbury Basin,

```
837 South Australia. Aust. J. Earth Sci., 72(2): 182-212, https://doi.org/10.1080/08120099.2025.2473098
```

- Castle-Jones, J., Betts, M.J., Jacquet, S.M., Chen, F., Zhang, Z., Hall, P.A., Klaebe, R.M. and Brock, G.A., 2025b. A new integrated lower cambrian chronostratigraphy for the normanville group, eastern stansbury basin, with definition of the oldest small shelly fossil zones in South Australia. Australasian Palaeontological Memoirs, 57: 465-489
 - Choubert, G., 1953. Le Précambrien III et le Géorgien de l'Anti-Atlas. In: P. Hupé (Editor), Contribution à l'étude du Cambrien inférieur et du Précambrien III de l'AntiAtlas marocain. Notes et Mémoires du Service Géologique du Maroc, 103: 7-39, pp. 7-39
 - Cohen, K.M., Finney, S.C., Gibbard, P.L. and Fan, J.X., 2013. The ICS International Chronostratigraphic Chart. International Union of Geological Sciences, 36(3): 199-204, https://doi.org/10.18814/epiiugs/2013/v36i3/002
 - Compston, W., Williams, I.S., Kirschvink, J.L., Zichao, Z. and Guogan, M.A., 1992. Zircon U-Pb ages for the Early Cambrian time-scale. Journal of the Geological Society, 149(2): 171-184, https://doi.org/10.1144/gsigs.149.2.0171
 - Cramer, B.D. and Jarvis, I., 2020. Chapter 11 Carbon Isotope Stratigraphy. In: F.M. Gradstein, J.G. Ogg, M.D. Schmitz and G.M. Ogg (Editors), Geologic Time Scale 2020. Elsevier, pp. 309-343, https://doi.org/10.1016/B978-0-12-824360-2.00011-5
 - Da Silva, A.C., De Vleeschouwer, D., Boulvain, F., Claeys, P., Fagel, N., Humblet, M., Mabille, C., Michel, J., Sardar Abadi, M., Pas, D. and Dekkers, M.J., 2013. Magnetic susceptibility as a high-resolution correlation tool and as a climatic proxy in Paleozoic rocks Merits and pitfalls: Examples from the Devonian in Belgium. Mar. Pet. Geol., 46: 173-189, http://dx.doi.org/10.1016/j.marpetgeo.2013.06.012
 - Da Silva, A.C., Triantafyllou, A. and Delmelle, N., 2023. Portable x-ray fluorescence calibrations: Workflow and guidelines for optimizing the analysis of geological samples. Chemical Geology, 623, https://doi.org/10.1016/j.chemgeo.2023.121395
 - Daley, A.C., Antcliffe, J.B., Drage, H.B. and Pates, S., 2018. Early fossil record of Euarthropoda and the Cambrian Explosion. Proc. Nat. Acad. Sci., 115(21): 5323, https://doi.org/10.1073/pnas.1719962115
 - De Winter, N.J., Sinnesael, M., Makarona, C., Vansteenberge, S. and Claeys, P., 2017. Trace element analyses of carbonates using portable and micro-X-ray fluorescence: performance and optimization of measurement parameters and strategies. Journal of analytical atomic spectrometry, 32(6): 1211-1223, https://doi.org/10.1039/C6JA00361C
 - Debrenne, F. and Debrenne, M., 1978. Archaeocyathid fauna of the lowest fossiliferous levels of Tiout (Lower Cambrian, Southern Morocco). Geol. Mag., 115(2): 101-119, https://doi.org/10.1017/S0016756800041157
 - Debrenne, F. and Debrenne, M., 1995. Archaeocyaths of the Lower Cambrian of Morocco. Beringeria(Special issue 2): 121-145
- Derry, L.A., Brasier, M.D., Corfield, R.M., Rozanov, A.Y. and Zhuravlev, A.Y., 1994. Sr and C isotopes in Lower Cambrian carbonates from the Siberian craton: A paleoenvironmental record during the 'Cambrian explosion'. Earth Planet. Sci. Lett., 128(3-4): 671-681, https://doi.org/10.1016/0012-821X(94)90178-3
- Dilliard, K.A., Pope, M.C., Coniglio, M., Hasiotis, S.T. and Lieberman, B.S., 2007. Stable isotope geochemistry of the lower Cambrian Sekwi Formation, Northwest Territories, Canada: Implications for ocean chemistry and secular curve generation. Palaeogeog. Palaeoclimatol. Palaeoecol., 256(3): 174-194, https://doi.org/10.1016/j.palaeo.2007.02.031
- dos Reis, M., Thawornwattana, Y., Angelis, K., Telford, M.J., Donoghue, P.J. and Yang, Z., 2015. Uncertainty in the timing of origin of animals and the limits of precision in

molecular timescales. Current Biology, 25(22): 2939-2950, https://doi.org/10.1016/j.cub.2015.09.066

893 894

895

898

899

900

901 902

903

904 905

906

907 908

911

912

913

914 915

916

917 918

- El Kabouri, J., Errami, E., Bowyer, F.T., Becker-Kerber, B. and Belkacim, S., 2025.

 Ediacaran-Cambrian Boundary in the Anti-Atlas belt (Morocco): A review of biostratigraphy, chemostratigraphy and geochronology. Earth Sci. Rev., 261: 105010, https://doi.org/10.1016/j.earscirev.2024.105010
 - Fan, R., Deng, S. and Zhang, X., 2011. Significant carbon isotope excursions in the Cambrian and their implications for global correlations. Science China Earth Sciences, 54(11): 1686-1695, https://doi.org/10.1007/s11430-011-4313-z
- Farhat, M., Auclair-Desrotour, P., Boué, G. and Laskar, J., 2022. The resonant tidal evolution of the Earth-Moon distance. A&A, 665: L1
 - Farrell, T.P., Cothren, H.R., Sundberg, F.A., Schmitz, M.D., Dehler, C.M., Landing, E., Karlstrom, K.E., Crossey, L.J. and Hagadorn, J.W., 2025. Revising the late Cambrian time scale and the duration of the SPICE event using a novel Bayesian age modeling approach. GSA Bulletin, https://doi.org/10.1130/b37919.1
 - Fritz, W.H., 1976. Ten stratigraphic sections from Lower Cambrian Sekwi Formation Mackenzie Mountains, northwestern Canada. Geological Survey of Canada, Paper 76-22: 41
 - Fu, D., Tong, G., Dai, T., Liu, W., Yang, Y., Zhang, Y., Cui, L., Li, L., Yun, H., Wu, Y., Sun, A., Liu, C., Pei, W., Gaines, R.R. and Zhang, X., 2019. The Qingjiang biota—A Burgess Shale–type fossil Lagerstätte from the early Cambrian of South China. Science, 363(6433): 1338-1342, https://doi.org/doi.10.1126/science.aau8800
- Geyer, G., 1989. Late Precambrian to early Middle Cambrian lithostratigraphy of southern
 Morocco. Beringeria, 1: 115-143
 - Geyer, G., 2019a. A comprehensive Cambrian correlation chart. International Union of Geological Sciences, 42(4): 321-332, https://doi.org/10.18814/epiiugs/2019/019026
 - Geyer, G., 2019b. The earliest known West Gondwanan trilobites from the Anti-Atlas of Morocco, with a revision of the Family Bigotinidae Hupé, 1953. Fossils and Strata, 64: 55-153
 - Geyer, G., 2019c. The earliest known West Gondwanan trilobites from the Anti-Atlas of Morocco, with a revision of the Family Bigotinidae Hupé, 1953, Papers from the 6th International Conference on Trilobites and their Relatives, pp. 55-153, https://doi.org/10.1002/9781119564249.ch6
- 920 Geyer, G. and Landing, E., 1995. The Cambrian of the Moroccan Atlas regions. Beringeria,, 921 2: 7-46
- Geyer, G. and Landing, E., 2006. Latest Ediacaran and Cambrian of the Moroccan Atlas
 regions. Beringeria Special Issue (6): 7-46
- Geyer, G. and Landing, E., 2018. An exploring expedition (sic) to the world's oldest trilobites,
 Proceedings of the International Conference on Ediacaran and Cambrian Sciences, pp.
 66-68
- Geyer, G. and Shergold, J., 2000. The quest for internationally recognized divisions of
 Cambrian time. International Union of Geological Sciences, 23(3): 188-195,
 https://doi.org/10.18814/epiiugs/2000/v23i3/006
- Harvey, T.H.P., Williams, M., Condon, D.J., Wilby, P.R., Siveter, D.J., Rushton, A.W.A.,
 Leng, M.J. and Gabbott, S.E., 2011. A refined chronology for the Cambrian succession
 of southern Britain. Journal of the Geological Society, 168(3): 705-716,
 https://doi.org/10.1144/0016-76492010-031
- Hollingsworth, J.S., 2005a. The earliest occurrence of trilobites and brachiopods in the Cambrian of Laurentia. Palaeogeog. Palaeoclimatol. Palaeoecol., 220(1): 153-165, https://doi.org/10.1016/j.palaeo.2004.08.008

- Hollingsworth, J.S., 2005b. The earliest trilobite in the Lower Cambrian ofwestern Laurentia
 and a suggested correlation for the base of a "trilobite-bearing" series. Acta
 Micropalaeontologica Sinica, 22 (Supplement): 59-60
- Hollingsworth, J.S., 2007. Fallotaspidoid trilobite assemblage from the Esmeralda Basin
 (western Nevada, U.S.A.). Memoirs of the Australasian Association of
 Palaeontologists, 32: 123-140

- Hollingsworth, J.S., 2011. Lithostratigraphy and biostratigraphy of Cambrian Stage 3 in western Nevada and eastern California. In: J.S. Hollingsworth, F.A. Sundberg and J.R. Foster (Editors), Cambrian Stratigraphy and Paleontology of Northern Arizona and Southern Nevada. Museum of Northern Arizona Bulletin, Flagstaff, Arizona, pp. 26–42.
- Holmes, J.D., Smith, P.M., Paterson, J.R., Brock, G.A. and Betts, M.J., 2025. The Cambrian Series 2–Miaolingian boundary interval in Australia: Biostratigraphic subdivision and implications for global multi-proxy correlation. Earth Sci. Rev., 265: 105106, https://doi.org/10.1016/j.earscirev.2025.105106
- Jamart, V., Pas, D., Adatte, T., Spangenberg, J.E., Laibl, L. and Daley, A.C., 2025. The Cambrian ROECE and DICE carbon isotope excursions in western Gondwana (Montagne Noire, southern France): Implications for regional and global correlations of the Miaolingian Series. Palaeogeog. Palaeoclimatol. Palaeoecol., 670: 112951, https://doi.org/10.1016/j.palaeo.2025.112951
- Kaufman, A.J. and Knoll, A.H., 1995. Neoproterozoic variations in the C-isotopic composition of seawater: stratigraphic and biogeochemical implications. Precambrian Research, 73(1): 27-49, https://doi.org/10.1016/0301-9268(94)00070-8
- Keppie, D.F., Keppie, J.D. and Landing, E., 2024. A tectonic solution for the Early Cambrian palaeogeographical enigma. In: R.D. Nance, R.A. Strachan, C. Quesada and S. Lin (Editors), Supercontinents, Orogenesis and Magmatism. Geological Society of London, pp. 0, https://doi.org/10.1144/sp542-2022-355
- Kirschvink, J.L., Magaritz, M., Ripperdan, R.L., Zhuravlev, A.Y. and Rozanov, A.Y., 1991. The Precambrian/Cambrian boundary: magnetostratigraphy and carbon isotopes resolve correlation problems between Siberia, Morocco, and South China. GSA today, 1(4): 69-91
- Kouchinsky, A., Bengtson, S., Clausen, S. and Vendrasco, M.J., 2015. An early Cambrian fauna of skeletal fossils from the Emyaksin Formation, northern Siberia. Acta Palaeontol. Polon., 60(2): 421-512, https://doi.org/10.4202/app.2012.0004
- Kouchinsky, A., Bengtson, S., Landing, E., Steiner, M., Vendrasco, M. and Ziegler, K., 2017. Terreneuvian stratigraphy and faunas from the Anabar Uplift, Siberia. Acta Palaeontol. Polon., 62(2): 311-44, https://doi.org10.4202/app.00289.2016
- Kouchinsky, A., Bengtson, S., Pavlov, V., Runnegar, B., Torssander, P., Young, E. and Ziegler,
 K., 2007. Carbon isotope stratigraphy of the Precambrian—Cambrian Sukharikha River
 section, northwestern Siberian platform. Geol. Mag., 144(4): 609-618,
 https://doi.org/10.1017/S0016756807003354
- Kouchinsky, A., Bengtson, S., Runnegar, B., Skovsted, C., Steiner, M. and Vendrasco, M.,
 2012. Chronology of early Cambrian biomineralization. Geol. Mag., 149(2): 221-251,
 https://doi.org/10.1017/S0016756811000720
- Landing, E., Antcliffe, J.B., Geyer, G., Kouchinsky, A., Bowser, S.S. and Andreas, A., 2018.
 Early evolution of colonial animals (Ediacaran Evolutionary Radiation—Cambrian
 Evolutionary Radiation—Great Ordovician Biodiversification Interval). Earth Sci. Rev.,
 178: 105-135, https://doi.org/10.1016/j.earscirev.2018.01.013
- Landing, E., Bowring, S.A., Davidek, K.L., Westrop, S.R., Geyer, G. and Heldmaier, W.,
 1998. Duration of the Early Cambrian: U-Pb ages of volcanic ashes from Avalon and

```
987 Gondwana. Canadian Journal of Earth Sciences, 35(4): 329-338, 
988 https://doi.org/10.1139/e97-107
```

994

995

1013

1014 1015

- Landing, E., Geyer, G., Brasier, M.D. and Bowring, S.A., 2013a. Cambrian Evolutionary
 Radiation: Context, correlation, and chronostratigraphy—Overcoming deficiencies of
 the first appearance datum (FAD) concept. Earth Sci. Rev., 123: 133-172,
 https://doi.org/10.1016/j.earscirev.2013.03.008
 - Landing, E., Geyer, G., Jirkov, I.A. and Schiaparelli, S., 2021a. Lophotrochozoa in the Cambrian evolutionary radiation and the Pelagiella problem. Papers in Palaeontology, 7(4): 2227-2244, https://doi.org/10.1002/spp2.1396
- Landing, E., Geyer, G., Westrop, S.R. and Smith, M., 2024. Trilobite Mineralization,
 diachronous lowest occurrences of trilobites, and global lower Cambrian subdivision
 standards. In: G.S.o.A.A.w. Programs (Editor), Geological Society of America Annual
 Meeting, https://doi.org/10.1130/abs/2024AM-402484
- Landing, E., Keppie, J.D., Keppie, D.F., Geyer, G. and Westrop, S.R., 2022. Greater

 Avalonia—latest Ediacaran—Ordovician "peribaltic" terrane bounded by continental
 margin prisms ("Ganderia," Harlech Dome, Meguma): Review, tectonic implications,
 and paleogeography. Earth Sci. Rev., 224: 103863,

 https://doi.org/10.1016/j.earscirev.2021.103863
- Landing, E., Schmitz, M.D., Geyer, G., Trayler, R.B. and Bowring, S.A., 2021b. Precise early
 Cambrian U–Pb zircon dates bracket the oldest trilobites and archaeocyaths in
 Moroccan West Gondwana. Geol. Mag., 158(2): 219-238,
 https://doi.org/10.1017/S0016756820000369
- Landing, E., Schmitz, M.D., Westrop, S.R. and Geyer, G., 2023. U-Pb zircon dates from
 North American and British Avalonia bracket the Lower–Middle Cambrian boundary
 interval, with evaluation of the Miaolingian Series as a global unit. Geol. Mag.,
 160(9): 1790-1816, https://doi.org/10.1017/S0016756823000729
 - Landing, E.D. and Kouchinsky, A., 2016. Correlation of the Cambrian Evolutionary Radiation: geochronology, evolutionary stasis of earliest Cambrian (Terreneuvian) small shelly fossil (SSF) taxa, and chronostratigraphic significance. Geol. Mag., 153(4): 750-756, https://doi.org/10.1017/S0016756815001089
- Landing, E.D., Westrop, S.R. and Bowring, S.A., 2013b. Reconstructing the Avalonia palaeocontinent in the Cambrian: A 519 Ma caliche in South Wales and transcontinental middle Terreneuvian sandstones. Geol. Mag., 150(6): 1022-1046, https://doi.org/10.1017/S0016756813000228
- Lantink, M.L., Davies, J.H.F.L., Ovtcharova, M. and Hilgen, F.J., 2022. Milankovitch cycles in banded iron formations constrain the Earth–Moon system 2.46 billion years ago.
 Proc. Nat. Acad. Sci., 119(40): e2117146119,
 https://doi.org/doi:10.1073/pnas.2117146119
- Laskar, J., 2020. Chapter 4 Astrochronology. In: F.M. Gradstein, J.G. Ogg, M.D. Schmitz
 and G.M. Ogg (Editors), Geologic Time Scale 2020. Elsevier, pp. 139-158,
 https://doi.org/10.1016/B978-0-12-824360-2.00004-8
- Laskar, J., Robutel, P., Joutel, F., Gastineau, M., Correia, A.C.M. and Levrard, B., 2004. A long-term numerical solution for the insolation quantities of the Earth. Astronomy and Astrophysics, 428(1): 261-285, https://doi.org/10.1051/0004-6361:20041335
- Latham, A. and Riding, R., 1990. Fossil evidence for the location of the
 Precambrian/Cambrian boundary in Morocco. Nature, 344(6268): 752-754,
 https://doi.org/10.1038/344752a0
- Li, M., Huang, C., Ogg, J., Zhang, Y., Hinnov, L., Wu, H., Chen, Z.-Q. and Zou, Z., 2019.

 Paleoclimate proxies for cyclostratigraphy: Comparative analysis using a Lower

- Triassic marine section in South China. Earth Sci. Rev., 189: 125-146, https://doi.org/10.1016/j.earscirev.2019.01.011
- Li, Z., Zhang, M., Chen, Z.-Q., Algeo, T.J., Zhao, L. and Zhang, F., 2021. Early Cambrian oceanic oxygenation and evolution of early animals: A critical review from the South China Craton. Global and Planetary Change, 204: 103561, https://doi.org/10.1016/j.gloplacha.2021.103561
- Liñán, E., Dies, M.E., Vintaned, J.A.G., Gozalo, R., Mayoral, E. and Muñiz, F., 2005. Lower
 Ovetian (Lower Cambrian) trilobites and biostratigraphy of the Pedroche Formation
 (Sierra de Córdoba, southern Spain). Geobios, 38(3): 365-381,

 https://doi.org/10.1016/j.geobios.2003.11.007
- Liñán, E., Gozalo, R., Dies Alvarez, M.E., Gamez Vintaned, J.A. and Zamora, S., 2008.
 Nuevos trilobites del Ovetiense inferior (Cámbrico Inferior bajo) de Sierra Morena
 (España). Ameghiniana, 45(1): 123-138
- Linnemann, U., Ovtcharova, M., Schaltegger, U., Gärtner, A., Hautmann, M., Geyer, G.,
 Vickers-Rich, P., Rich, T., Plessen, B., Hofmann, M., Zieger, J., Krause, R., Kriesfeld,
 L. and Smith, J., 2019. New high-resolution age data from the Ediacaran–Cambrian
 boundary indicate rapid, ecologically driven onset of the Cambrian explosion. Terra
 Nova, 31(1): 49-58, https://doi.org/10.1111/ter.12368
- Magaritz, M., Holser, W.T. and Kirschvink, J.L., 1986. Carbon-isotope events across the Precambrian/Cambrian boundary on the Siberian Platform. Nature, 320(6059): 258-259, https://doi.org/10.1038/320258a0
- Magaritz, M., Kirschvink, J.L., Latham, A.J., Zhuravlev, A.Y. and Rozanov, A.Y., 1991.
 Precambrian/Cambrian boundary problem: Carbon isotope correlations for Vendian and Tommotian time between Siberia and Morocco. Geology, 19(8): 847-850, https://doi.org/10.1130/0091-7613
- Maloof, A., Ramezani, J., Bowring, S., Fike, D., Porter, S. and Mazouad, M., 2010.
 Constraints on early Cambrian carbon cycling from the duration of the Nemakit Daldynian–Tommotian boundary δ13C shift, Morocco. Geology, 38(7): 623-626,
 http://dx.doi.org/10.1130/G30726.1
 - Maloof, A.C., Schrag, D.P., Crowley, J.L. and Bowring, S.A., 2005. An expanded record of Early Cambrian carbon cycling from the Anti-Atlas Margin, Morocco. Canadian Journal of Earth Sciences, 42(12): 2195-2216, https://doi.org/10.1139/e05-062
- Mángano, G.M. and Buatois, L.A., 2017. The Cambrian revolutions: Trace-fossil record,
 timing, links and geobiological impact. Earth Sci. Rev., 173: 96-108,
 https://doi.org/10.1016/j.earscirev.2017.08.009
- Marshall, C.R., 2006. Explaining the Cambrian "Explosion" of Animals. Annu. Rev. Earth
 Planet. Sci., 34(1): 355-384, https://doi.org/10.1146/annurev.earth.33.031504.103001
- Martinez, M., Kotov, S., De Vleeschouwer, D., Pas, D. and Pälike, H., 2016. Testing the impact of stratigraphic uncertainty on spectral analyses of sedimentary series. Climate of the Past, 12(9): 1765-1783, http://doi.org/10.5194/cp-12-1765-2016
- McKerrow, W.S., Scotese, C.R. and Brasier, M.D., 1992. Early Cambrian continental
 reconstructions. Journal of the Geological Society, 149(4): 599-606,
 https://doi.org/10.1144/gsjgs.149.4.0599
- Merdith, A.S., Williams, S.E., Collins, A.S., Tetley, M.G., Mulder, J.A., Blades, M.L., Young,
 A., Armistead, S.E., Cannon, J., Zahirovic, S. and Müller, R.D., 2021. Extending fullplate tectonic models into deep time: Linking the Neoproterozoic and the Phanerozoic.
 Earth Sci. Rev., 214: 103477, https://doi.org/10.1016/j.earscirev.2020.103477
- 1083 Meyers, S., 2014. Astrochron: An R Package for Astrochronology

1067

Meyers, S.R., 2019. Cyclostratigraphy and the problem of astrochronologic testing. Earth Sci. Rev., 190: 190-223, https://doi.org/10.1016/j.earscirev.2018.11.015

- Moczydłowska, M., 1998. Cambrian acritarchs from Upper Silesia, Poland biochronology
 and tectonic implications, Cambrian acritarchs from Upper Silesia, Poland biochronology and tectonic implications. Fossils and Strata, 46, pp. 1-121,
 https://doi.org/10.18261/8200376923-1998-01
- Moczydłowska, M. and Zang, W.-L., 2006. The Early Cambrian acritarch Skiagia and its significance for global correlation. Palaeoworld, 15(3-4): 328-347, https://doi.org/10.1016/j.palwor.2006.10.003
- Monninger, W., 1979. The section of Tiout (Precambrian/Cambrian boundary beds, Anti-Atlas, Morocco): An environmental model, Würzburg, Arb. Paläont. Inst. Würzburg, 1, , 289 pp
- Pas, D., Elrick, M., Da Silva, A.-C., Hinnov, L., Jamart, V., Thaureau, M. and Arts, M., 2024.

 Millennial-scale climate cycles modulated by Milankovitch forcing in the middle
 Cambrian (ca. 500 Ma) Marjum Formation, Utah, USA. Geology, 52(8): 605-609,

 https://doi.org/10.1130/g52182.1
- Pas, D., Hinnov, L., Day, J.E., Kodama, K., Sinnesael, M. and Liu, W., 2018.
 Cyclostratigraphic calibration of the Famennian stage (Late Devonian, Illinois Basin, USA). Earth Planet. Sci. Lett., 488: 102-114, https://doi.org/10.1016/j.epsl.2018.02.010
- Paterson, J.R., Edgecombe, G.D. and Lee, M.S.Y., 2019. Trilobite evolutionary rates constrain the duration of the Cambrian explosion. Proc. Nat. Acad. Sci., 116(10): 4394-4399, https://doi.org/10.1073/pnas.1819366116
- Peng, S. and Babcock, L.E., 2011. Continuing progress on chronostratigraphic subdivision of the Cambrian system. Bull. Geosci., 86(3): 391-396, https://doi.org/10.3140/bull.geosci.1273
- Peng, S., Babcock, L.E. and Cooper, R.A., 2012. The Cambrian Period, The Geologic Time Scale 2012, pp. 437-488, https://doi.org/10.1016/B978-0-444-59425-9.00019-6
- Peng, S.C., Babcock, L.E. and Ahlberg, P., 2020. Chapter 19 The Cambrian Period. In: F.M. Gradstein, J.G. Ogg, M.D. Schmitz and G.M. Ogg (Editors), Geologic Time Scale 2020. Elsevier, pp. 565-629, https://doi.org/10.1016/B978-0-12-824360-2.00019-X
- Porter, S.M., 2007. Seawater Chemistry and Early Carbonate Biomineralization. Science, 316(5829): 1302-1302, https://doi.org/doi:10.1126/science.1137284
- Potin, G.J.-M. and Daley, A.C., 2023. The significance of Anomalocaris and other Radiodonta for understanding paleoecology and evolution during the Cambrian explosion.

 Frontiers in Earth Science, 11, https://doi.org/10.3389/feart.2023.1160285
- Pruss, S.B. and Gill, B.C., 2024. Life on the Edge: The Cambrian Marine Realm and Oxygenation. Annu. Rev. Earth Planet. Sci., 52: 109-132, https://doi.org/10.1146/annurev-earth-031621-070316
- 1123 Ramsey, C., 2009. Bayesian Analysis of Radiocarbon Dates. Radiocarbon, 51(1): 337-360, https://doi.org/10.1017/S0033822200033865
- 1125 Rozanov, A.Y., Khomentovsky, V.V., Shabanov, Y.Y., Karlova, G.A., Varlamov, A.I.,
 1126 Luchinina, V.A., Pegel, T.V., Demidenko, Y.E., Parkhaev, P.Y., Korovnikov, I.V. and
 1127 Skorlotova, N.A., 2008. To the problem of stage subdivision of the Lower Cambrian.
 1128 Stratigr. Geol. Correl., 16(1): 1-19, https://doi.org/10.1007/s11506-008-1001-3
- Rozanov, A.Y., Parkhaev, P.Y., Demidenko, Y.E. and Skorlotova, N., 2011. Mobergella radiolata—a possible candidate for defining the base of Cambrian Series 2 and Stage 3. Museum of Northern Arizona Bulletin, 67: 304-306
- Saadi, S., Hilali, E., Bensaïd, , M., B., A., and Dahmani, M., 1985. Carte Géologique de
 Maroc 1/1,000,000. Notes et Mémoirs de la Service Géologique du Maroc 260.
 Ministère de l'Énergie et des Mines, Direction de la Géologie, Rabat.

- Schoenemann, B., Pärnaste, H. and Clarkson, E.N.K., 2017. Structure and function of a compound eye, more than half a billion years old. Proc. Nat. Acad. Sci., 114(51): 13489-13494, https://doi.org/doi:10.1073/pnas.1716824114
- Scotese, C.R., 2021. An Atlas of Phanerozoic Paleogeographic Maps: The Seas Come In and the Seas Go Out. Annu. Rev. Earth Planet. Sci., 49: 679-728, https://doi.org/10.1146/annurev-earth-081320-064052
- 1141 Sdzuy, K., 1978. The Precambrian–Cambrian boundary beds in Morocco (Preliminary 1142 Report). Geol. Mag., 115(2): 83-94, https://doi.org/10.1017/S0016756800041133

1147

1148

11581159

1160

1161

11621163

1164

1165

1166

- Sdzuy, K. and Geyer, G., 1988. The base of the Cambrian in Morocco. In: V.H. Jacobshagen

 (Editor), The Atlas System of Morocco: Studies on Its Geodynamic Evolution: Lecture

 Notes in Earth Sciences. Springer-Verlag, pp. 91-106
 - Sdzuy, K., Liñán, E. and Gozalo, R., 1999. The Leonian Stage (early Middle Cambrian): a unit for Cambrian correlation in the Mediterranean subprovince. Geol. Mag., 136(1): 39-48, https://doi.org/10.1017/S0016756899002241
- Shergold, J.H. and Geyer, G., 2003. The Subcommission on Cambrian Stratigraphy: the status quo. Geologica Acta, 1: 5-9, https://doi.org/10.1344/105.000001588
- Sinnesael, M., De Vleeschouwer, D., Zeeden, C., Batenburg, S.J., Da Silva, A.-C., de Winter, N.J., Dinarès-Turell, J., Drury, A.J., Gambacorta, G., Hilgen, F.J., Hinnov, L.A., Hudson, A.J.L., Kemp, D.B., Lantink, M.L., Laurin, J., Li, M., Liebrand, D., Ma, C., Meyers, S.R., Monkenbusch, J., Montanari, A., Nohl, T., Pälike, H., Pas, D., Ruhl, M., Thibault, N., Vahlenkamp, M., Valero, L., Wouters, S., Wu, H. and Claeys, P., 2019. The Cyclostratigraphy Intercomparison Project (CIP): consistency, merits and pitfalls. Earth Sci. Rev., 199: 102965, https://doi.org/10.1016/j.earscirev.2019.102965
 - Sinnesael, M., Millard, A.R. and Smith, M.R., 2024. A Bayesian astrochronology for the Cambrian first occurrence of trilobites in West Gondwana (Morocco). Geology, 52(3): 205-209, https://doi.org/10.1130/g51718.1
 - Steiner, M., Li, G. and Ergaliev, G., 2011. Toward a subdivision of the traditional 'Lower Cambrian'. Museum of Northern Arizona Bulletin, 67: 306-308
 - Torsvik, T.H. and Cocks, L.R.M., 2016. Cambrian. In: T.H. Torsvik and L.R.M. Cocks (Editors), Earth History and Palaeogeography. Cambridge University Press, Cambridge, pp. 85-100, https://doi.org/10.1017/9781316225523.006
 - Tucker, M.E., 1986. Carbon isotope excursions in Precambrian/Cambrian boundary beds, Morocco. Nature, 319(6048): 48-50, https://doi.org/10.1038/319048a0
- Varlamov, A.I., Rozanov, A.Y., Khomentovsky, V.V., Shabanov, Y.Y., Abaimova, G.P.,
 Demidenk, Y.E., Karlova, G.A., Korovnikov, I.V., Luchinina, V.A.m., Malakhovskaya,
 Y., Parkhaev, P.Y., Pegel, T.V., Skorlotova, N.A., Sundukov, V.M., Sukhov, S.S.,
 Fedorov, A.B. and Kipriyanova, L.D.e., 2008. The Cambrian System of the Siberian
 Platform. Part 1: The Aldan–Lena Region, PIN RAS Moscow-Novosibirsk, pp. 295 pp
- Waltham, D., 2015. Milankovitch period uncertainties and their impact on cyclostratigraphy.

 J. Sediment. Res., 85(8): 990, https://doi.org/10.2110/jsr.2015.66
- Wood, R. and Erwin, D.H., 2018. Innovation not recovery: dynamic redox promotes metazoan radiations. Biological Reviews, 93(2): 863-873, https://doi.org/10.1111/brv.12375
- Wood, R., Zhuravlev, A.Y. and Debrenne, F., 1992. Functional biology and ecology of Archaeocyatha. Palaios, 7(2): 131-156, https://doi.org/10.2307/3514925
- Wu, Y.J., Malinverno, A., Meyers, S.R. and Hinnov, L.A., 2024. A 650-Myr history of Earth's axial precession frequency and the evolution of the Earth-Moon system derived from cyclostratigraphy. Science Advances, 10(42), https://doi.org/10.1126/sciadv.ado2412
- Yang, B., Chen, D. and Liu, M., 2025. Integrating sequence and carbon isotope stratigraphy in the lower Cambrian (Stage 3), Tarim Basin: Implications for stratigraphic correlation

1184	and environmental-biotic evolution. Palaeogeog. Palaeoclimatol. Palaeoecol., 667:				
1185	112881, https://doi.org/10.1016/j.palaeo.2025.112881				
1186	Yang, C., Li, XH., Zhu, M., Condon, D.J. and Chen, J., 2018. Geochronological constraint				
1187	on the Cambrian Chengjiang biota, South China. Journal of the Geological Society,				
1188	175(4): 659-666, https://doi.org/10.1144/jgs2017-103				
1189	Young, G.M., 2015. Environmental upheavals of the Ediacaran period and the Cambrian				
1190	"explosion" of animal life. Geoscience Frontiers, 6(4): 523-535,				
1191	https://doi.org/10.1016/j.gsf.2014.09.001				
1192	Zhang, T., Li, Y., Fan, T., Da Silva, AC., Shi, J., Gao, Q., Kuang, M., Liu, W., Gao, Z. and				
1193	Li, M., 2022a. Orbitally-paced climate change in the early Cambrian and its				
1194	implications for the history of the Solar System. Earth Planet. Sci. Lett., 583: 117420,				
1195	https://doi.org/10.1016/j.epsl.2022.117420				
1196	Zhang, T., Li, Y., Fan, T., Da Silva, A.C., Kuang, M., Liu, W., Ma, C., Gao, Q., Shi, J., Gao, Z.				
1197	and Li, M., 2022b. Orbital forcing of tropical climate dynamics in the Early Cambrian.				
1198	Global and Planetary Change, 219, https://doi.org/10.1016/j.gloplacha.2022.103985				
1199	Zhang, X., Ahlberg, P., Babcock, L.E., Choi, D.K., Geyer, G., Gozalo, R., Hollingsworth, J.S.,				
1200	Li, G., Naimark, E.B., Pegel, T., Steiner, M., Wotte, T. and Zhang, Z., 2017.				
1201	Challenges in defining the base of Cambrian Series 2 and Stage 3. Earth Sci. Rev.,				
1202	172: 124-139, https://doi.org/10.1016/j.earscirev.2017.07.017				
1203	Zhao, Z., Thibault, N.R., Dahl, T.W., Schovsbo, N.H., Sørensen, A.L., Rasmussen, C.M.Ø.				
1204	and Nielsen, A.T., 2022. Synchronizing rock clocks in the late Cambrian. Nature				
1205	Communications, 13(1): 1990, https://doi.org/10.1038/s41467-022-29651-4				
1206	Zhu, M., Yang, A., Yuan, J., Li, G., Zhang, J., Zhao, F., Ahn, SY. and Miao, L., 2019.				
1207	Cambrian integrative stratigraphy and timescale of China. Science China Earth				
1208	Sciences, 62(1): 25-60, https://doi.org/10.1007/s11430-017-9291-0				
1209	Zhu, M.Y., Babcock, L.E. and Peng, S.C., 2006a. Advances in Cambrian stratigraphy and				
1210	paleontology: Integrating correlation techniques, paleobiology, taphonomy and				
1211	paleoenvironmental reconstruction. Palaeoworld, 15(3-4): 217-222,				
1212	https://doi.org/10.1016/j.palwor.2006.10.016				
1213	Zhu, M.Y., Babcock, L.E. and Peng, S.C., 2006b. Advances in Cambrian stratigraphy and				
1214	paleontology: Integrating correlation techniques, paleobiology, taphonomy and				
1215	paleoenvironmental reconstruction. Palaeoworld, 15(3-4 SPEC. ISS.): 217-222,				
1216	https://doi.org/10.1016/j.palwor.2006.10.016				
1217	Zhu, M.Y., Zhang, J.M., Li, G.X. and Yang, A.H., 2004. Evolution of C isotopes in the				
1218	Cambrian of China: Implications for Cambrian subdivision and trilobite mass				
1219	extinctions. Geobios, 37(2): 287-301, https://doi.org/10.1016/j.geobios.2003.06.001				
1220					
1221					
1222	8. Figures				

9. Figures

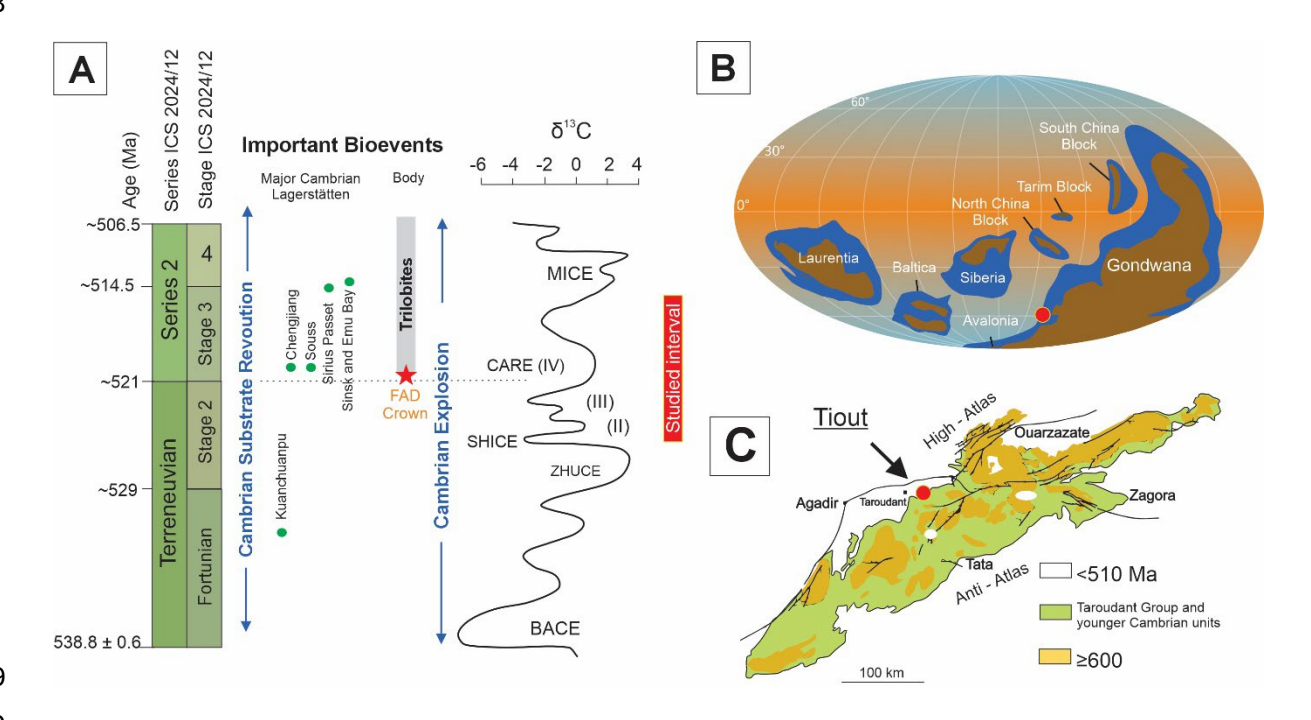


Fig. 1. Early Cambrian global composite δ¹³C curve, biological and environmental events, paleogeographic location, and stratigraphic interval covered in this study (Marshall, 2006; Zhu et al., 2006b; Daley et al., 2018; Peng et al., 2020; Pruss and Gill, 2024). (**B**) Global Early Cambrian paleogeography showing the location of the study area (red dot) West Gondwana, modified from (Torsvik and Cocks, 2016; Merdith et al., 2021; Scotese, 2021). A paleogeographic alternative (Landing et al., 2022; Keppie et al., 2024) uses climate indicators (Adoudou Formation evaporites, carbonate platform development and archaeocyath reefs in the Igoudine and Amouslek) and rotation of Gondwana to place the Moroccan margin in the tropics, with Avalonia, separated from Gondwana and Baltica the only temperate paleocontinents. (**C**) geological map modified after Saadi et al. (1985) showing the Tiout study area within the western edge of the Anti-Atlas. Ad., Adoudou Formation. Note that the Taroudant Group records the Basal Cambrian carbon isotope Excursion (BACE).

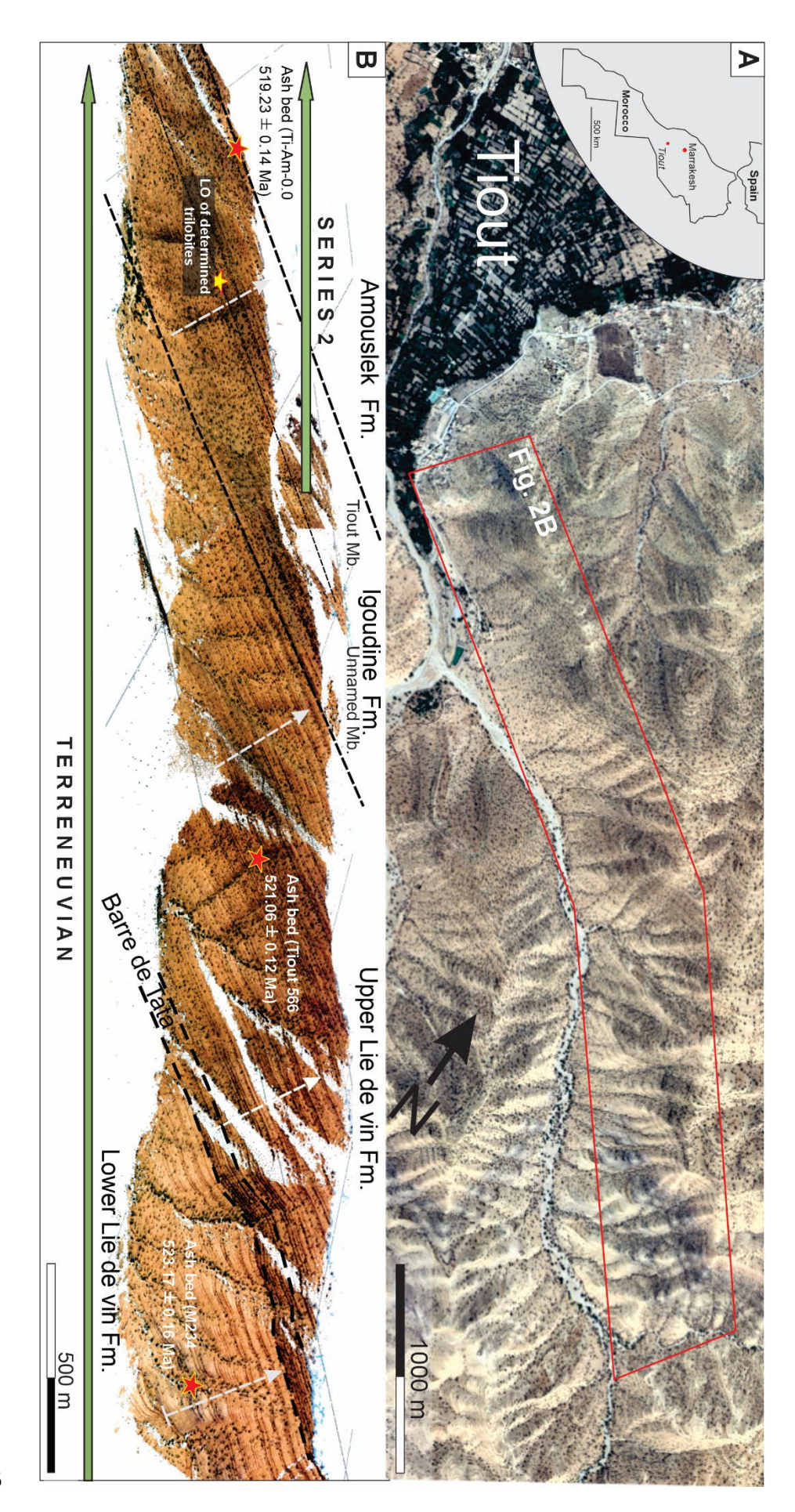


Fig. 2. Overview of the Tiout section. (**A**) Map of the study area (Tiout, Morocco) showing the section measured along the Oued irrigating the Tiout oasis. (**B**) Complete stratigraphic interval studied in Tiout (for location see inset in Fig. 2A) based on integration of multiple drone photographs. The figure shows the location of dated ash layers (Ti Am0.0, Ti-566 and M234), Formation and members boundaries from the terminal Terreneuvian to the early Cambrian Series 2. White dashed arrows represent a synthetic view of the measured stratigraphy (see Supplementary Figures 2 to see the location of each measured and sampled intervals in more detail).

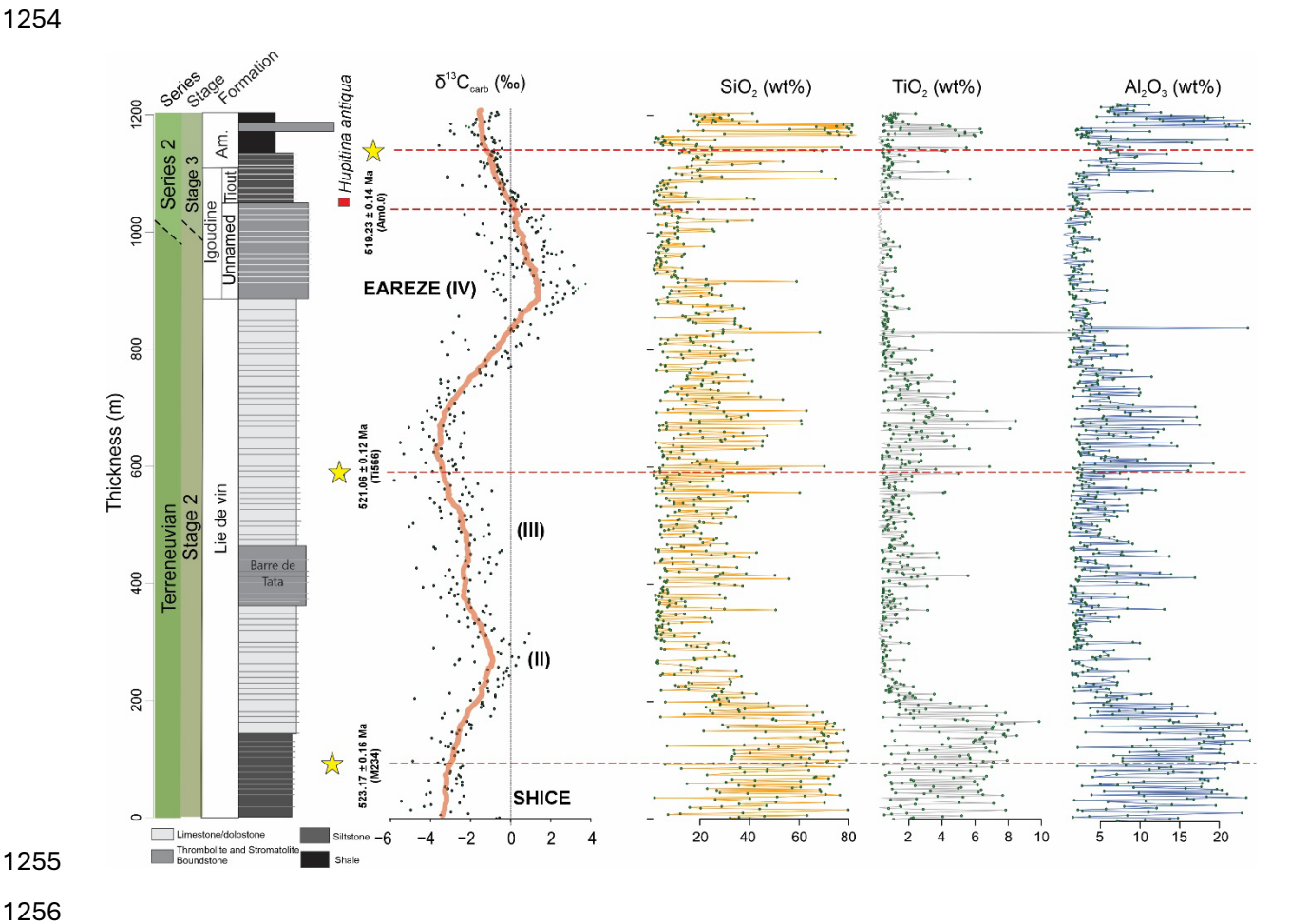


Fig. 3. Sedimentological versus chemostratigraphic profiles for the Tiout section with location of dated ash beds, the LO of identified trilobites and carbon isotope excursions (SHICE, excursion II and III and EAREZE (IV) are shown. Chemostratigraphic profiles include the $\delta^{13}C_{carb}$ (with corresponding 35 point moving average) and pXRF-derived detrital proxies SiO₂, Al₂O₃, K₂O assumed to represent detrital input delivery into the marine realm.

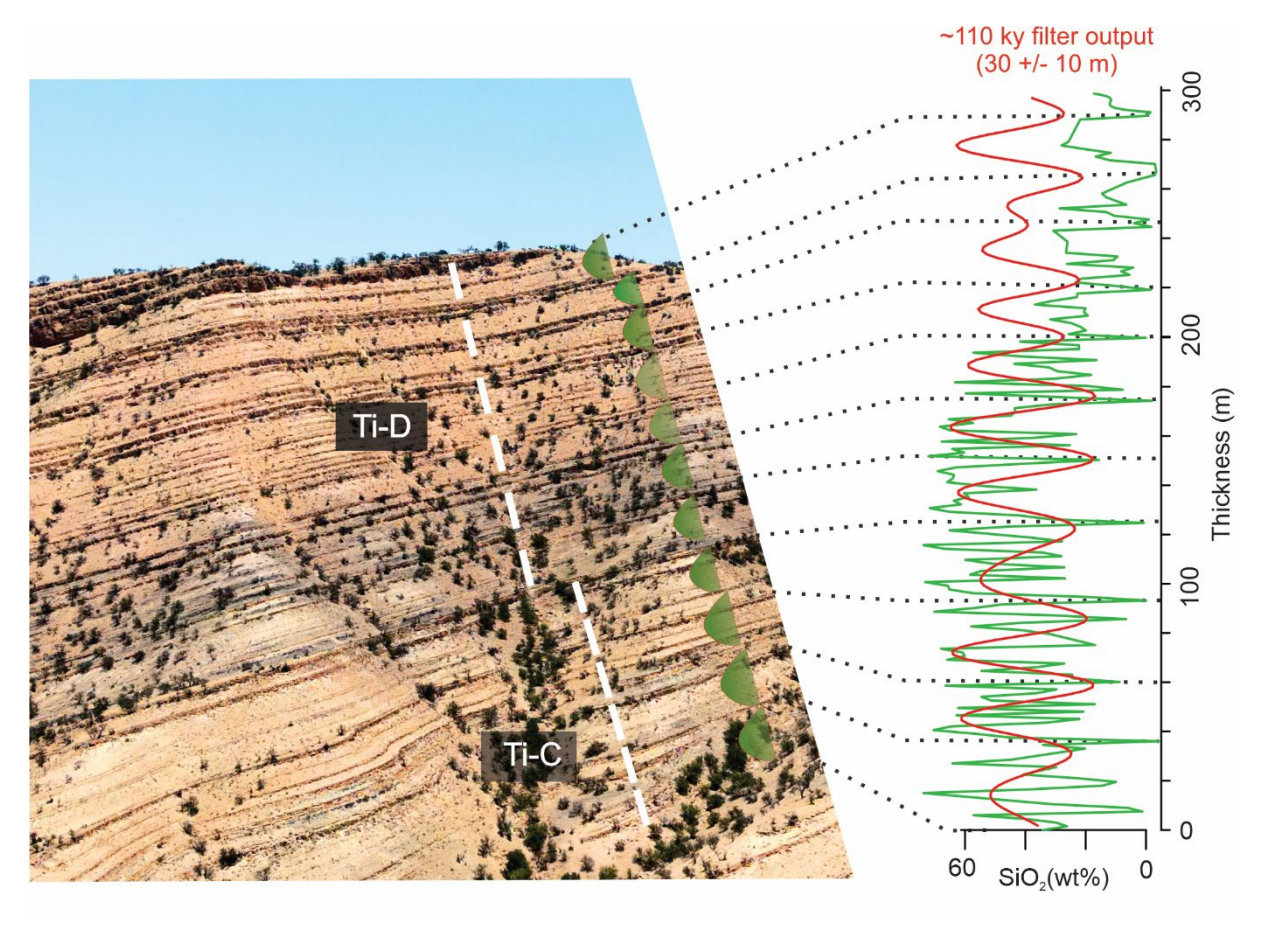


Fig. 4. Weathering versus SiO₂ profile in the lower Lie de vin Formation showing that elevated SiO₂ concentrations consistently coincide with marlstone-rich or highly weathered intervals at cyclothem scale (20–40 m). Ti-D and Ti-C and white dashed lines refer to sampled interval names used in this study (see supplementary materials for details).

Pas et al. – Main text 36

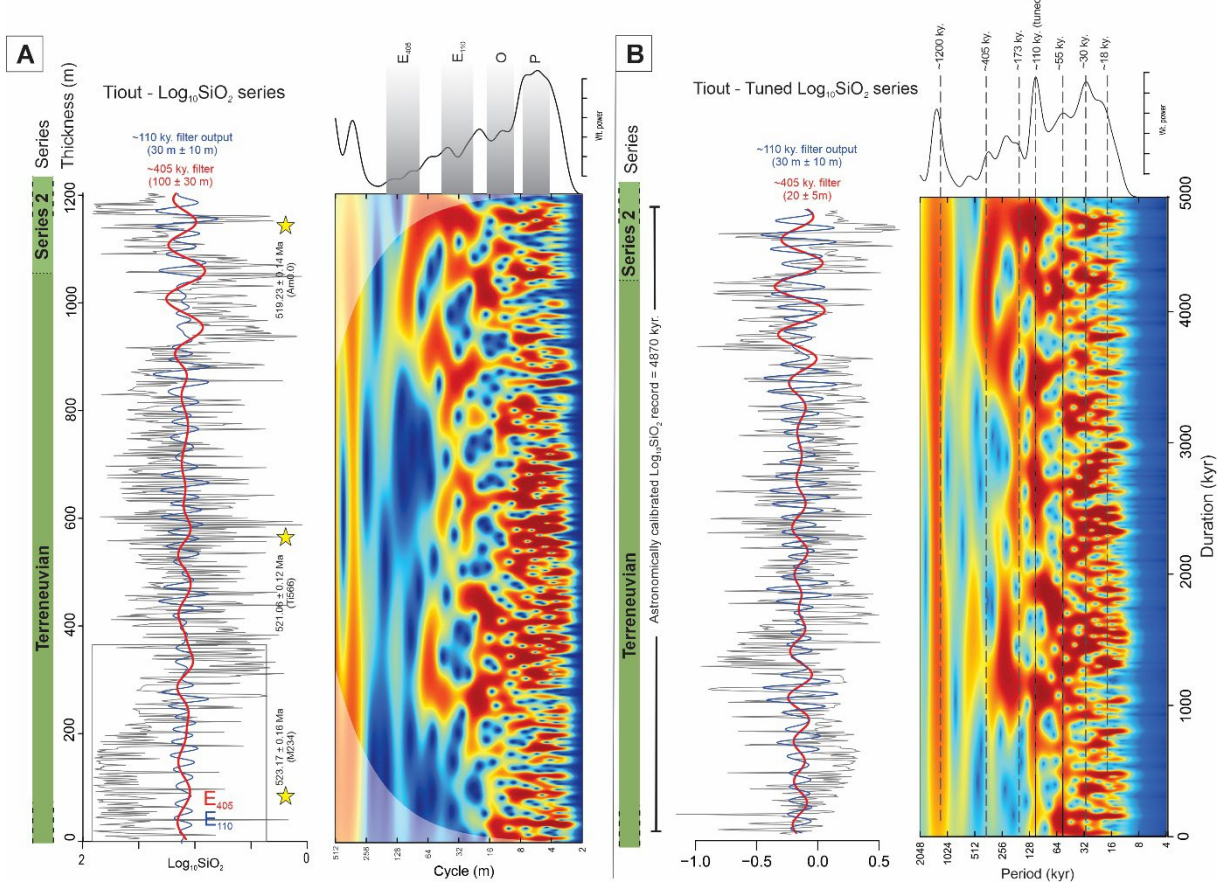


Fig. 5. (**A**) \log_{10} SiO₂ stratigraphic series with interpreted 405 kyr (E₄₀₅; red), 110 kyr (E₁₁₀; blue) Taner-filtered output series and location of dated ash beds (Astrochron; Meyers, 2014). CWT analysis (Arts, 2023) showing main wavelength bands expected for the Tiout section when considering that short eccentricity cycle is expressed in a 20–40 m windows. Bands are approximately ~74–147 m for the long eccentricity (405 kyr), ~5.8–11.6 m for the obliquity (~32 kyr), and ~3.3–6.7 m for precession (~18.3 kyr). These estimates are based on the predicted early Cambrian astronomical frequency ratios (22.13:3.6:1) (Laskar et al., 2004; Waltham, 2015; Farhat et al., 2022). (**B**) Short eccentricity (110 kyr) tuned \log_{10} SiO₂ series showing the 405 kyr (red), and 110 kyr (blue) Taner-filtered output and corresponding CWT with peak power at ~1200 kyr, ~405 kyr, ~173 kyr. ~110 kyr (tuned), ~55 kyr, ~30 kyr and ~18 kyr. Astronomical calibration for the Tiout section provides a duration estimate of 4870 ± 110 kyr.

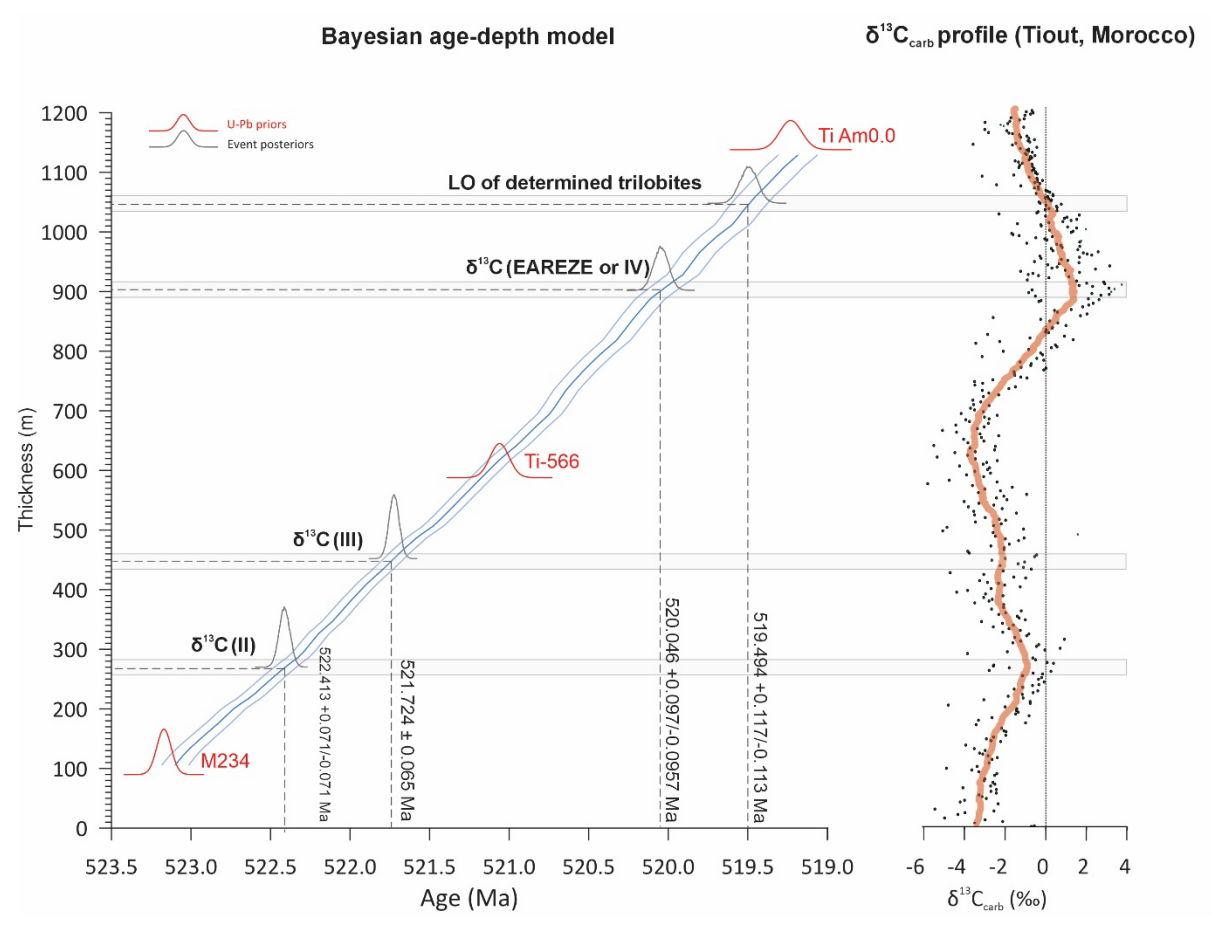
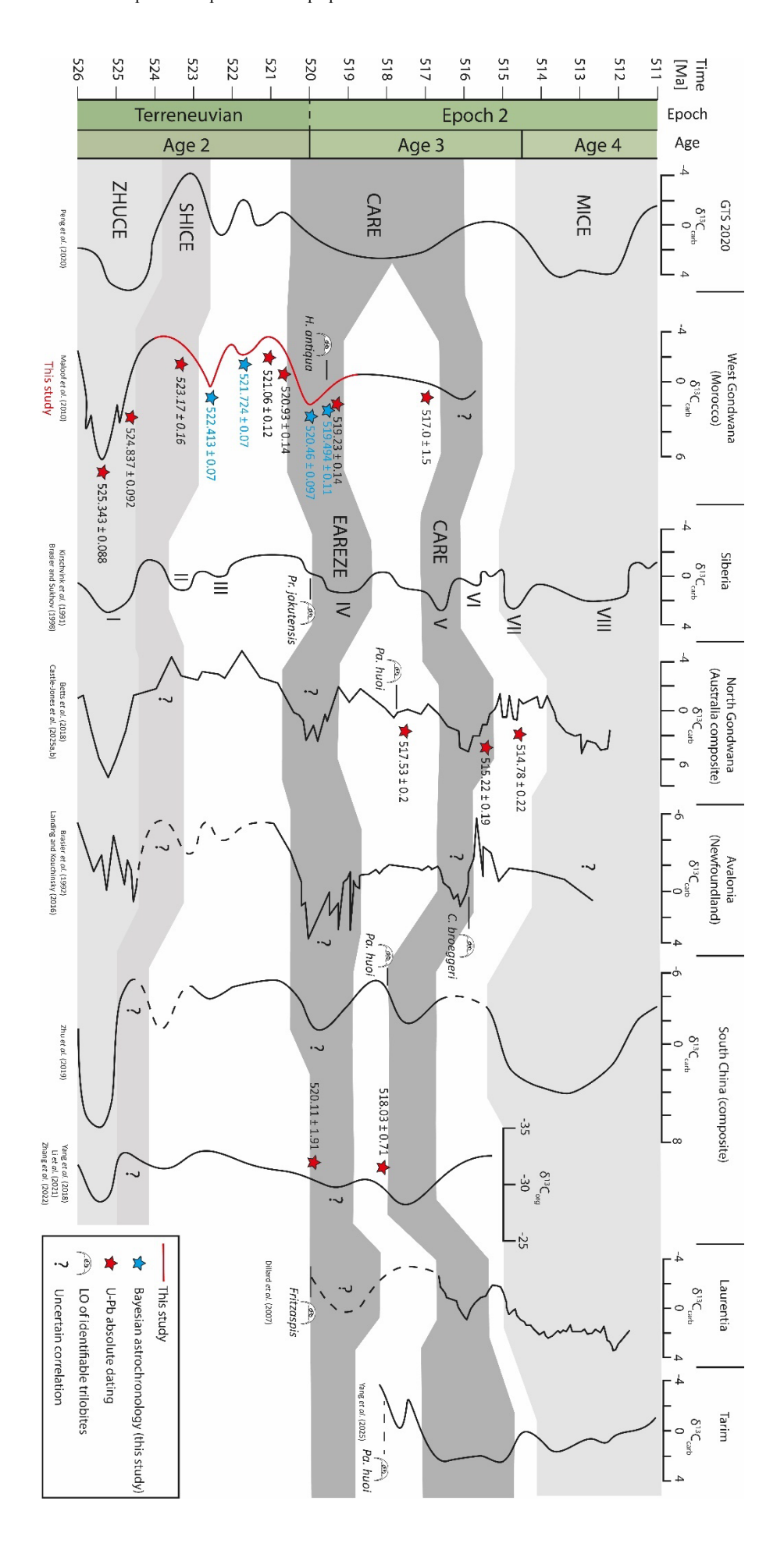


Fig. 6. Bayesian age modeling resulting from Our OxCal age-depth models for the Tiout section, Morocco against the $\delta^{13}C_{carb}$ profile. The integration of new astrochronological information from this study with the available U-Pb radioisotope age constraints provides age estimates for the several biogeochemical events within the lower Cambrian in West Gondwana. The depth scale is calculated in function of cycles depth for plotting. HPD—highest posterior distribution.

Pas et al. – Main text 38



. . . .

Fig. 7. Proposed global correlation scheme for the EAREZE and CARE. Tarim (Yang et al., 2025), Laurentia (Dilliard et al., 2007), South China (Yang et al., 2018; Zhu et al., 2019; Li et al., 2021; Zhang et al., 2022b), Avalonia (Brasier et al., 1992), North Gondwana (Australia composite) (Betts et al., 2018; Castle-Jones et al., 2025a; Castle-Jones et al., 2025b), Siberia (Kirschvink et al., 1991; Brasier and Sukhov, 1998), West Gondwana (Morocco)(Maloof et al., 2010). Abbreviation: C. – Callavia, H. – Hupetina, Pa. – Parabadiella, Pr. – Profallotaspis

Position in the Tiout composite section (m)	Event	Likelihood age (Ma, ±95% confidence interval)	Posterior age (Ma, ±95 HPD)	Formation/Member
88.5	Ash M234 equivalent	523.17 ± 0.16		Lie de vin/Lower
270	Excursion III		522.413 +0.071/-0.070	Lie de vin/Lower
453	Excursion III		521.72 +0.065/-0.065	Lie de vin/Lower
556.5	Ash Ti-566	521.06 ± 0.12		Lie de vin/Upper
901.5	EARZE (IV)		520.046 +0.097/-0.0957	Igoudine/Unnamed
1017.2	Trolobites sclerites		519.62 +0.11/-0.11	Igoudine/Unnamed
1048.3	LO of H. antiqua		519.494 +0.117/-0.113	Igoudine/Tiout
1062.9	LO Archeocyaths		519.44 +0.117/-0.113	Igoudine/Tiout
1137	Ti-Am0.0	519.23 ± 0.14		Amouslek

Table 1. Bayesian astrochronology age results for the composite Tiout section (Anti-Atlas,

1320 Morocco)